muscle related peptides.
Results: LC-MS/MS gave peptide profiles containing 60 proteins consistent with a variety of fast and slow twitch muscle proteins as well as numerous general muscle protein markers. 12 of 37 proteins identified by IHC were specific to fast twitch muscle (most abundant proteins being beta-enolase and fast skeletal myosin light chain 2) and 6 of 26 proteins identified by negative IHC were specific to slow twitch muscle (most abundant proteins being myosin light chain 3 and myosin regulatory light chain 2). General muscle markers, such as myoglobin, were observed in both stained and unstained cells.
Conclusions: Our study shows that detailed proteomic analysis can be successfully performed on IHC stained tissue sections. Using this methodology, the proteome of single muscle cells can be identified and subtle differences in protein expression between physiological subsets of skeletal muscle can be demonstrated. As this technology is readily applicable to routine clinical biopsy specimens, it is likely that LC MS/MS-based proteomic analysis will have wide ranging applications in biomarker discovery and clinical diagnosis.

1711 Phosphoscan Analysis of Mantle Cell Lymphoma Cell Lines

A Zamo, TL Gu, RD Polakiewicz, A Parisi, A Bertolaso, S Barbi, G Inghirami, F Menestrina. University of Verona, Verona, Italy; Cell Signaling Technology, Inc., Danvers, MA; University of Torino, Turin, Italy.
Background: Mantle cell lymphoma (MCL) constitutes about 5% of non-Hodgkin lymphoma in the western world. It shows a characteristic clinical behaviour with initial response to therapy followed by relapses and death in 3-5 years. Many studies have investigated MCL pathogenesis by high-throughput techniques such as gene expression profiling, but very few have attempted the study of MCL from a proteomic point of view. In our previous work, we have focused our attention on the phospho-proteome of several MCL cell lines by IMAC pre-fractionation and 2D-PAGE/MS.
Design: In this work we used the PhosphoScan approach, which has already been successfully used in the phospho-profiling of lung cancer and acute myeloid leukemia. This involves a protein extraction followed by a digestion. Phosphorylated peptides are then immunoprecipitated by anti-phosphotyrosine antibody followed by capillary electrophoresis and MS identification of eluted peptides. We analysed four MCL cell lines (MAVER-1, Jeko-1, Rec-1 and Granta-519).
Results: 421 unique peptides were identified, corresponding to 341 proteins. Of these, 191 were present in at least two cell lines, and were further analysed for KEGG pathway. This analysis showed that the most represented ones are "Regulation of actin cytoskeleton" (16 proteins, 9.04%), "Focal adhesion" (15 proteins, 8.47%), "Fc epsilon RI signaling pathway" (14 proteins, 7.91%) and "B cell receptor signaling pathway" (13 proteins, 7.34%). The four pathways are strongly interconnected, and suggest the activation of the B-cell receptor in these cell lines. The absence of the antigen during in vitro culture suggests that these cell have a tonic BCR signalling either by abnormalities of the signalling pathway or by self-stimulation.
Conclusions: The BCR signalling pathway is promising from a therapeutic point of view, and recent data indicate that it might be very important in the pathogenesis of DLBCL. Its importance in MCL has not been investigated so far. PhosphoScan analysis of MCL cell lines suggests that tonic BCR signalling might be one of the mechanisms driving cell survival and proliferation in MCL, but these data need to be validated by functional studies and by the extensive analysis of tissue samples.

1712 TMPRSS2 Gene Rearrangement in Non-Prostatic Epithelial Tumors

C Zanardi, J Tull, S Zhang, C Fuller. SUNY Upstate Medical University, Syracuse, NY.
Background: Transmembrane serine protease 2 (TMPRSS2) is an androgen-regulated member of the type two transmembrane protease family (TTSP) that is normally expressed to a variable degree in prostate, colon, stomach, liver, testicle, kidney and pancreas. The TMPRSS2 (21q22.3) gene has been recently observed to be fused with several of the ETS-transcription factor family members, including ERG (21q22.2), ETV1 (7q21.2) or ETV4 (17q21), in a significant percentage of prostate carcinomas. The current study was undertaken to determine whether TMPRSS2 gene rearrangements are detectable in other common non-prostatic epithelial tumors.
Design: Tissue microarrays (TMA) were constructed to contain duplicate or triplicate cores of 164 cases of a variety of carcinomas from the following sites: breast, head and neck region including thyroid and salivary gland, lung, pleura, liver, pancreas, skin, adrenal gland, and gastrointestinal, gynecological, and urogenital systems. These TMAs were then subjected to direct fluorescence in situ hybridization (FISH) using a bacterial artificial chromosome (BAC)-derived TMPRSS2 gene dual-color break-apart probe cocktail. A positive result was reported when greater than 10% of the tumor nuclei had evidence of split red and green signals, indicative of TMPRSS2 gene rearrangement. A parallel analysis of TMAs containing prostate carcinomas was used for comparison.
Results: All tested non-prostatic epithelial tumor cases showed very rare or no tumor cell nuclei with split FISH signals, confirming an intact TMPRSS2 gene region in these tumors. In contradistinction, 62% of tested prostate carcinomas harbored demonstrable TMPRSS2 gene rearrangements.
Conclusions: These findings demonstrate absence of TMPRSS2 gene rearrangements in an extensive sampling of non-prostatic epithelial tumors, supporting the concept that TMPRSS2 alterations are unique and specific to carcinomas of prostatic origin. More comprehensive screening of similar large cohorts of epithelial tumors will be necessary to determine the incidence of rearrangements of ETS family members involving alternate fusion partner genes or other novel gene rearrangements in non-prostatic epithelial tumors.

1713 The Use of Itraq and Mass Spectrometry To Study Multiple Myeloma Associated with Bortezomib Resistance

JH Zhao, J Chen, K Evans, H Chang. University Health Network and University of Toronto, Toronto, Canada.
Background: Bortezomib, a novel proteasome inhibitor, represents a promising new clinical strategy presently deployed in clinical trials of relapsed and refractory multiple myeloma (MM). However, only 30-40% of MM patients respond to this treatment. The mechanism of resistance is not understood. Our previous study on the molecular cytogenetic profiles of MM showed that the response to bortezomib in MM patients is independent of high-risk genomic aberrations. In order to gain insights into the mechanisms of bortezomib resistance, we examined the proteome of bortezomib sensitive and resistant MM cells by comparative global proteomic analysis.
Design: Two myeloma cell lines, 8226/S (bortezomib senbsitive) and 8226/R5 (bortezomib resistance) were used in this study to determine differentially expressed proteins possibly directly involved in the acquisition of bortezomib resistance. The proteins of bortezomib sensitive and resistant cells were simultaneously identified and quantified by using isobaric tag peptide labeling (iTRAQ) technology, followed by hybrid quadruple time-of-flight mass spectrometry (MS). The MS based multiple-reaction-monitoring (MRM) technique was used to independently verify the quantitative differences of the protein expression levels between the two cell lines.
Results: The iTRAQ labeling combined with MS approach identified a large population of 665 proteins from MM cells. Among those proteins, 176 proteins (27%) were found differentially expressed between 8226/S and 8226/R5. Of the 176 proteins, 115 (65%) were up-regulated whereas 61 (35%) were down-regulated. These proteins can be classified into several major cellular pathways involving cell proliferation, differentiation, nuclear acid metabolism, molecular transport and protein synthesis. Several selected highly expressed proteins such as DEN1C, Ubiqulin-4, SCFD1 may be considered as potential protein biomarkers for bortezomib resistance.
Conclusions: iTRAQ in concert with MS is a powerful approach to identify differentially expressed proteins related to drug resistance in MM. Further verification and functional analysis of the proteins of interest in MM bortezomib resistance are ongoing.

Techniques

1714 Dermatopathology in the Digital Era

A Al Habeeb, D Ghazarian. UHN, Toronto, ON, Canada; Timmins Hospital, Timmins, ON, Canada.
Background: Teledermatopathology has the potential to deliver quality service to underserviced areas. Our airms are: To validate teledermatopathology as a diagnostic tool in underserviced areas To test its utilization in inflammatory and melanocytic lesions To compare the impact of 20x and 40x resolution on diagnostic accuracy.
Design: A total of 103 cases were studied. Routine skin cases (n=79) from Timmins were scanned at 20x using aperio 5 slides scanscope. A pathologist diagnosed these cases using light microscopy. Subsequently, these were provided to a UHN pathologist along with the information on the requisition . The pathologist was blinded to the diagnoses. Additional 12 cases of inflammatory skin biopsies (IS)and 12 melanocytic lesions (ML) were scanned at 20x and 40x with an emphasis on assessing objective findings. For IS, these findings were divided into three main columns: epidermal, dermal and other findings. For ML, benign and malignant cases were mixed and objective findings were evaluated utilizing epidermal, and dermal attributes. The quality of picture was assessed in a scale from 1-3 (1=inferior, 2= similar, and 3= superior quality compared to light microscope). The UHN pathologist was blinded to the clinical information and the final diagnoses.The assessment started with the 20x proceeding to 40x.
Results: The concordance rate for the routine cases scanned from Timmins was (96%). There were 3 minor discrepancies in 3 cases (Intradermal nevus vs. compound nevus, actinic keratosis vs. in-situ squamous cell carcinoma, and seborrheic keratosis vs. verruca vulgaris). These discrepancies were thought to represent judgment bias rather than a function of picture resolution. All the inflammatory skin findings corresponded to the original report except one case where leukocytoclastic vasculitis was originally reported but was not recorded by the UHN pathologist though it was suggested. There was a focus in the original slide that was lost in the scanned recut slide. The 20x scanned slides were given a score of 2 each, however, 40x scanned slides were given a score of 3.The melanocytic lesions showed 100% concordence rate in both the 20x and 40x. However, in malignant and atypical melanocytic lesions 40x gave a superior resolution with detailed nuclear features and easier pick up of mitoses.
Conclusions: Teledermatopathology can serve as a primary and a second opinion diagnostic tool with a potential for expansion to underserviced areas to deliver quality service. Scanning at 40x is superior to 20x particularly in inflammatory and atypical melanocytic lesions.

1715 Gene Expression Profiling of Peripheral Blood during In Vitro Fertilisation Treatment Reveals Predictive Markers of Pregnancy

C Allen, CM Martin, JJ O'Leary. Rotunda Hospital, Dublin, Ireland; Coombe Women's Hospital, Dublin, Ireland.
Background: Infertility is an increasing global disease but the molecular pathways surrounding human conception remain poorly understood. There are no reliable predictors of success for invasive fertility treatments. Here we examine the functional transcriptome in IVF induced pregnancy and non-pregnant controls, to elucidate predictive biomarkers which identify implantation events, maintenance of pregnancy, and pregnancy outcome.
Design: Gene expression patterns in RNA extracted from peripheral blood at time points during IVF cycles from 5 women who achieved clinical pregnancies, 3 women who had implantation failure, and 3 subfertile women who conceived spontaneously

were evaluated. Total RNA was extracted from whole blood collected in Tempus™ RNA collection Tubes using the ABI PRISM™ 6100 Nucleic Acid PrepStation. Gene expression analysis was performed using AB Human Genome Survey Microarrays. Data analysis was performed using R statistical package, molecular function and biological process analysis was performed using Panther.

Results: 128 genes were differentially expressed in early pregnancy compared with a non-pregnant state ($p < 0.05$). Associated molecular pathways include angiogenesis, endothelin signaling, inflammation, oxidative stress, VEGF, and pyruvate metabolism. 200 genes were differentially expressed at a pre-treatment time-point in women who became pregnant compared to those who did not ($p<0.05$). Associated molecular pathways include angiogenesis, blood coagulation, endogenous cannabiniod, inflammation, and Wnt signaling pathway. Transcripts associated with cysteine biosynthesis were differentially expressed in the early post-conceptual period in the pregnant women compared to those with implantation failure. 237 genes were differentially expressed in first trimester IVF conceptions compared with spontaneous conceptions in subfertile women ($p<0.05$). Associated molecular pathways include Heterotrimeric G protein signaling.

Conclusions: This is the first report of gene expression profiles in peripheral blood during in vitro fertilization. The transcriptome signature for early human pregnancy is influenced by the trimera of mother, fetus, and placenta. Gene expression profiles prior to IVF are predictive of outcome, and could aid clinical decision-making for future patients. Significant differences in gene expression between assisted and natural conceptions is of concern and highlights the need to optimize IVF protocols.

1716 Use of Whole Slide Imaging for Tissue Microarrays: The Cooperative Prostate Cancer Tissue Resource Model

W Amin, IZ Yildiz Aktas, J Duboy, T Harper, H Singh, JT Milnes, R Deaton, V Macias, A Kajdacsy-Balla, MJ Becich, AV Parwani. University of Pittsburgh, Pittsburgh, PA; University of Pittsburgh Medical Center, Pittsburgh, PA; University of Illinois at Chicago, Chicago, IL.

Background: The NCI Cooperative Prostate Cancer Tissue Resource (CPCTR) is a virtual tissue bank comprised of four academic centers with archived thousands of clinically annotated prostate cancer specimens and six well characterized paraffin embedded Tissue Microarrays (TMAs) to fulfill the needs of the oncology research community. In order to enhance value to these collections, the CPCTR TMAs have been imaged using virtual microscopy and whole slide imaging of the glass slides with a link to the annotated de-identified patient data.

Design: The Whole Slide Imaging (WSI) Facility at our institution runs several high-throughput imagers (Aperio, Zeiss, Hamamatsu). A full time imaging technician is employed for monitoring and maintenance of the system and image QA. The CPCTR WSI project is accomplished in three major steps: 1) Collection of all glass slides used for TMA construction from the collaborating CPCTR sites. The H&E slides pen-marking of tumor areas where the cores were extracted from and sent for image capture along with slides; 2) Scanning the whole donor slides at 20 X and the TMA slide at 40 X magnification with Aperio ScanScopes at both institutions followed by downloading of images into an image server; and 3) Building internet links between each tissue core in a TMA map, the corresponding whole slide image and TMA core image.

Results: After automated image capture, the imaging technician visually examined whole slide images for image quality and a pathologist reviewed of the images. The scanned images were then linked to the TMA maps. It provides high-quality and well annotated images to the researchers. Additionally, this can allow the CPCTR imaging project to function effectively across academic institutions and represent a virtual bank with images. In total 18 slides of 5 TMAs have been scanned.

Conclusions: Significant advancement in WSI technology allows to routinely image large numbers of slides automatically, rapidly and at high resolution. The CPCTR TMA imaging provides a digital image bank functions effectively across the academic institutions and represents a virtual bank with clinical annotation to facilitate translational research.

1717 Quantitative Evaluation of the Protein Expression as a Function of Tissue Microarray Core Diameter: Is a Large (1.5mm) Core Better Than a Small (0.6mm) One?

VK Anagnostou, FJ Lowery, KN Syrigos, DL Rimm. Yale University School of Medicine, New Haven, CT.

Background: Tissue microarrays (TMAs) have emerged as a robust, high-throughput technology for protein evaluation in large cohorts and clinical biomarker development. This technique allows maximization of tissue resources by analysis of sections from small core (0.6-1.5mm in diameter) "biopsies" of standard formalin fixed, paraffin embedded tissue blocks. This allows processing of hundreds of cases arrayed on a single recipient block in an identical manner. Although pathologists frequently choose larger core sizes, there is no evidence in the literature showing that larger cores are better (or worse) than small cores for assessment of TMAs.

Design: We assessed the expression of a series of conventional biomarkers (ER, HER2, EGFR, STAT3, mTOR and phospho p70 S6K) by immunofluorescence using AQUA® for protein measurement within subcellular compartments on a continuous scale. One random 0.6mm field (one 0.6 mm spot) was compared to 6-12 fields per spot representing 1mm and 1.5 mm cores in 4 different tumor types.

Results: We showed that measurement of a single random 0.6mm spot was comparable to analysis of the whole 1mm or 1.5 mm spot (Pearson's R coefficient varying from 0.87-0.98) for all markers tested.

Conclusions: Although this study does not test markers that may be at lower density, like micro-vessel counts or cell subsets (ie macrophages), we conclude that for standard protein markers expressed in epithelial tumors, 0.6mm cores are equally representative as compared to any larger core size. Since TMA technology is now being used in all phases of biomarker development, this work suggests that 0.6mm cores are optimal since more cores can be arrayed in a single master block and the use of this core size allows increased throughput and decreased cost.

1718 Expression of Melanoma Markers in Plasma Cell Dyscrasias (PCD): A Possibility for Misdiagnosis

MK Atieh, GA Barkan, EM Wojcik, S Alkan. Loyola University Medical Center, Maywood, IL.

Background: Plasma cells have not been known to express melanocytic markers such as S100 and Melan-A/Mart-1. Due to a recent case of a plasmacytoma mimicking a melanoma (morphologically as well as immunohistochemically) in a patient with history of melanoma, we have pursued the current study to evaluate the potential ability of neoplastic plasma cells to express melanocytic markers.

Design: A retrospective database search was performed for PCD (plasmacytoma (P) or multiple myeloma (MM)) from 1998 to 2007. Only patients with a documented diagnosis of a PCD were included. A total of 37 cases were used in this study, (5-P, 32-MM). The patients ages ranged from 28 to 89 years (mean= 52.5 years) with 54% being male, and 46% female. Tissue microarray blocks were made from the paraffin embedded tissue using 4-mm cores. Slides from these tissue microarray blocks were stained with H&E, S100 and Melan-A/Mart-1. Staining intensity was graded as negative, 1+, 2+, and 3+ when compared to the control slides. Zero and 1+ staining were noted as negative, 2+ and 3+ staining were noted as positive.

Results: Analysis of the immunohistochemical stains in plasma cells showed that 5/37 cases (13.5 %) exhibited a diffuse staining pattern with strong cytoplasmic positivity for both S100 and Melan-A/Mart-1. Of these, 4/5 (80%) were from patients that had a diagnosis of multiple myeloma; 1/5 (20%) had a diagnosis of plasmacytoma.

Plasma Cell Expression Of Melanoma Antigens

	S100(n,%)	Melan-A/Mart-1(n,%)
NEGATIVE	32(86.5%)	32(86.5%)
1+	0(0%)	0(0%)
2+	3(8.1%)	1(2.7%)
3+	2(5.4%)	4(10.8%)

Conclusions: It can be difficult to render a diagnosis of a PCD in a patient with a history of malignant melanoma when complicated by atypical plasma cell morphology with expression of aberrant melanoma antigens. We have shown that 13.5% of PCD express S100 and Melan-A/Mart-1. If the suspicion for a PCD is high, other immunohistochemical stains (CD 138 and kappa/lambda light chain) and additional modalities should be utilized to rule out such a diagnosis. The current study aims to alert practicing pathologists to this potential pitfall that they may encounter in their daily practice.

1719 A Real Time PCR Assay for the Detection of the GSTP1 Single Nucleotide Polymorphism A313G

ML Baker, AL Marchetti, CL Bartels, JM Pipas, CE Fadul, GJ Tsongalis. Dartmouth Medical School, Dartmouth Hitchcock Medical Center and Norris Cotton Cancer Center, Lebanon, NH.

Background: GSTP1 is a member of the glutathione-S-transferase multigene family, and is a cytosolic enzyme responsible for catalyzing the metabolism and detoxification of xenobiotic agents via conjugation with glutathione. The single-nucleotide polymorphism A313G (Ile105Val) is known to alter substrate affinity of GSTP1 via steric restriction, and is associated with variations in GSTP1 metabolic activity. This study evaluates a real-time PCR assay for detection of the A313G SNP.

Design: In this study we utilized DNA samples from 40 de-identified Caucasian patients who had been previously tested for other genetic disorders to assess the specificity of an allelic discrimination assay (TAQman™ SNP Genotyping Assay C_3237198, ABI Assays-on-Demand) using the ABI 7500 FAST real time PCR system. DNA from these samples was isolated using the Qiagen EZ1 Robotic workstation. In addition, DNA was extracted from 24 formalin-fixed, paraffin-embedded tissue sections from colon cancer specimens to determine if this assay would perform on archived materials. This assay utilized the following: ABI 2X FAST universal master mix, 10-20 ng of genomic DNA in a total reaction volume of 10 µl using the default fast cycling conditions. A post amplification plate read was used for allelic discrimination according to the ABI 7500 user manual.

Results: Of 40 Caucasian DNA samples, 13 (32.5%) were homozygous for the A allele, 19 (47.5%) were heterozygous for A/G, and 8 (20%) were homozygous for the G allele. This corresponds to the frequency data presented in the NCI SNP500 database (http://snp500cancer.nci.nih.gov). Of 24 colon cancer cases, the following distribution was observed: 11/24 (45.8%) were homozygous for the A allele, 12/24 (50%) were heterozygous for A/G, and 1/24 (4%) was homozygous for the G allele.

Conclusions: Our study suggests that the ABI 7500 FAST TAQman™ SNP Genotyping Assay is suitable for differentiating the "A" from the "G" alleles in clinical DNA samples arising from whole blood or archived tissues. Real time PCR thermocycling capabilities have resulted in a very robust TAQman™ assay that has the advantage of improved turn-around-time and throughput.

1720 Immunohistochemistry Improves the Diagnostic Accuracy of Intrauterine Gestation in the Examination of Products of Conception

SM Bakhiet, J Fahy, JF Gillan. Rotunda Hospital/TCD, Dublin, Ireland.

Background: The detection of chorionic villi in products of conception is crucial for diagnosing intrauterine gestation. In the absence of villi, intrauterine implantation can be diagnosed, by the presence of intermediate trophoblast. Gursan et al (2002) introduced anti-Cytokeratin as a marker for intermediate trophoblasts in such cases. The use of a panel of immunostains has not been widely studied. In addition, the role of deeper levels has not however been previously described in the literature as an alternative method for detecting chorionic villi.

Design: To further characterize the immunocytochemical features of intermediate trophoblast and to possibly identify a more sensitive marker, a conventional H&E deeper level in addition to a panel immunostains for AE 1/3, hPL and hCG were performed in 81 endometrial specimens from patients with first trimesteric miscarriage (suspected intra-uterine gestations) that lacked chorionic elements (Goup1). Endometrial specimens from 5 patients with known intrauterine gestation (Group 2), 5 patients with known Ectopic pregnancy (Group 3) and 5 patients with non-pregnant status (Group 4) were used as positive and negative controls respectively.
Results: Of 81 specimens of product of conception examined, all specimens did not show any chorionic villi on original histological examination however microscopic examination of deeper levels from these specimen showed 10/81 (12.35%) of cases having chorionic villi that didn't appear on the original H&E slides. Intermediate trophoblast in vessels and/or decidua was difficult to recognized by conventional light microscopy in all the test cases however it was identified by immunoperoxidase reactions for keratin in 44/81 (54.32%), hPL in 21/81 (25.93%) and hCG in 16/81 (19.75%) of these cases. Controls:- Group 2 showed 100 positivity, Group 3 and Group 4 were all negative. Cytokeratin AE 1/3 stained also the endometrial glands and occasional suspected single or clustered epithelial cells. This cross-reaction may potentially mislead the unwary. This was overcome with hPL/hCG stains, which proved negative in these settings.
Conclusions: This study reveals that combined Cytokeratin AE 1/3, hPL and hCG immunostains increases diagnostic yields. Cytokeratin is a very sensitive and reliable however we recommend using hPL and hCG in addition to Cytokeratin as markers to avoid false positive results.

1721 Adopting Automated Gel Testing in a Small Community Hospital Blood Bank: More Positive Antibody Screens and Failure to Accurately Type a Rare cisAB Genotype

RD Boyum, MA Brooks, JS Luster, BI Ruiz. Naval Hospital Pensacola, Pensacola, FL.
Background: Automation is the primary advantage of using gel testing techniques rather than traditional tube testing in transfusion service laboratories. However, the performance characteristics of automated gel testing are not the same as those for traditional tube testing, and adopting this new technology poses unique challenges for small community hospital blood banks. We report an analysis of the first 13 months of automated gel technology use, to replace traditional tube testing, in a small community (US Navy) hospital.
Design: For data collected between April 1, 2006 and April 30, 2007, ABO/Rh typing, antibody screens, and antibody identification were performed using traditional tube testing with low ionic strength solution (LISS). For data collected between May 1, 2007 and June 30, 2008, ABO/Rh typing and antibody screens were performed using the Provue™ (Ortho-Clinical Diagnostics) automated gel testing system; antibody identifications were performed by a reference laboratory (Northwest Florida Blood Services, Pensacola, FL) using tube testing with low ionic strength solution (LISS) and polyethylene glycol (PEG).
Results: Of 2284 antibody screens performed with gel testing, 83 (3.63%) were positive, 42 (1.84%) were positive due to passively acquired anti-D (RhIg injection), and 20 (24.10% of all positive screens) had no antibody detected on confirmatory testing. Of 1606 antibody screens performed with tube testing, 31 (1.93%) were positive, 15 (0.93%) were positive due to passively acquired anti-D (RhIg injection), and 2 (6.45% of all positive screens) had no antibody detected on confirmatory testing. Antibody screening with automated gel testing detected a single case of anti-E, a clinically significant alloantibody, three months before it was detected and identified by tube testing. Automated gel testing failed to detect B antigen expressed by a rare cisAB genotype. When the same sample was testing using manual gel or traditional tube techniques, the B antigen was detected.
Conclusions: In comparison to traditional tube testing, automated gel testing apparently has increased sensitivity for the detection of both clinically insignificant (anti-D due to RhIg injection) and clinically significant (anti-E due to alloimmunization) antibodies. In contrast, automated gel testing has apparently decreased sensitivity for the detection of B-antigen expressed in a patient with a rare cisAB genotype; this decreased sensitivity was not seen with manual gel testing.

1722 Under Vacuum Preservation of Tissues To Be Transferred to Pathology Labs

G Bussolati, L Chiusa, A Cimino, G D'Armento. University of Turin, Turin, Italy.
Background: Tissue specimens to be transferred from the surgical theatres to the pathology labs are usually immersed in formalin, used as a preserver and fixative. This procedure prevents fresh tissue collection for tissue banking and involves the handling of formalin (a toxic and carcinogenic agent) by nurses in the surgical theatre. Indeed, it is now regarded as mandatory to try to reduce exposure to formalin.
Design: To overcome these problems, we adopted an under-vacuum (U.V.) processing for large specimens (while small biopsies are directly immersed in formalin in pre-filled containers). An under-vacuum machine ("Tissue-safe"®, by Milestone, Bergamo, Italy) was located in the surgical theatres in our Hospital. Immediately after removals, specimens were put in a plastic bag and processed under-vacuum (the whole processing is lasting less than 1 min.), then kept in a fridge at 4°C until transferred to the Pathology Lab. In the grossing room, the specimens were processed as usual. To test the safety and efficacy of the procedure, we have been checking the preservation of histological features, of antigen detectability and of nucleic acid integrity in tissues kept U.V. for various times (from a few hours up to 5 days).
Results: The experience accrued on over 1000 cases (mainly of breast, thyroid, colon lesions) processed Under-vacuum and sent to the Pathology Lab. for grossing allows to conclude that this processing is well appreciated by both nurses and laboratory personnel. Fresh U.V. tissues kept in the fridge (4°C) up to 2-3 days still retain an excellent morphology, as well as preservation of (immunohistochemically detectable) antigens and of nucleic acids. Tissues banking, cell coltures and electron microscopy were still feasible in such material. This procedure offers advantages in the processing of breast biopsies.
Conclusions: Tissues transfer in under-vacuum conditions meets the request of health authorities and involved personnel to reduce exposure to formaldehyde, while safely preserving in tissues both morphological and biological features of diagnostic interest.

1723 Rapid Automated DNA/RNA Extraction: Validation of Quick Gene 810 (QG) for Blood and Tissue Specimen Processing

M Cankovic, J Beher, L Whiteley, RJ Zarbo, D Chitale. Henry Ford Hospital, Detroit, MI.
Background: Molecular Pathology is a rapidly growing area offering many tests. Testing is performed on a variety of samples such as peripheral blood, bone marrow, formalin fixed paraffin embedded (FFPE) tissue etc. Therefore there is a growing need for automation, high throughput, random access in method of nucleic acid extraction. We report our experience with the Fuji Film QG, a bench-top DNA/RNA isolation instrument (AutoGen,Holliston,MA).
Design: QG and manual DNA extraction protocols (QIAampDNA Mini Kit, Qiagen, Valencia,CA) were run in parallel for genomic DNA from 12 blood specimens (WBC 4.9-9.9 x 10^6/mL) and 12 FFPE tissues-colon(3), breast(2), lung (2), prostate(2), kidney(1), skin(2). QG and manual protocols (5 Prime,Gaithersburg,MD) were used to isolate total RNA from blood and the QG and TrimGen Wax Free (TrimGen,Sparks,MD) from FFPE tissues. DNA/RNA quantity were evaluated by spectrophotometry. DNA integrity was assessed by amplification of Control Size Ladder mix (InVivo Scribe,San Diego,CA) generating a series of amplicons. RNA integrity was assessed by real-time quantitative reverse transcription PCR by measurement of expression of β2 microglobulin (B2M) transcripts, with acceptable cycle threshold (Ct) values of 30 for blood and 35 for FFPE tissues run in duplicates.
Results: Extraction times were shorter by QG for Blood DNA/RNA. Manually isolated FFPE DNA was of superior quality. Both methods gave amplifiable DNA from blood and FFPE. Blood RNA from both methods was amplifiable, but the manually extracted samples gave lower Ct values. For tissue RNA, Ct was at background for 10/12 samples for QG, compared to Ct 24.95 to 32.39 for manual extraction.

Results

	QG-BLOOD	MANUAL-BLOOD	QG-FFPE	MANUAL-FFPE
DNA extraction time	10 min	40 min	60 min	74 min
Mean DNA purity	1.75(1.63-2.0)	1.71(1.42-1.93)	1.10(0.69-2.81)	2.05(1.5-2.3)
DNA integrity	Good	Good	Good	Good
RNA extraction time	39 min	45 min	60 min	74 min
Mean RNA purity	1.46(0.74-2.72)	1.19(0.75-2.46)	0.26(0.00-3.85)	1.15(1.0-1.3)
RNA integrity	Fair	Good	Failure 10/12	Good

Conclusions: QG was easy to incorporate into the lab and is suited for small to medium throughput laboratories. The greatest time and cost savings were with DNA isolations from blood (30 minutes and $15 /sample). Blood RNA and tissue DNA protocols didn't yield substantial time savings, but were still cost effective due to elimination of several manual steps. Tissue RNA quality was suboptimal with QG in our experience.

1724 Detection and Quantitation of EGFR Gene Copy Number/ Amplification by FISH in Non-Small Cell Lung Cancer (NSCLC) – A Comparative Study with IHC Stains in 537 Cases

S Chopra, B Shahbahrami, T Cheng, M Gu. Oncotech Inc., Tustin, CA; University of California Irvine Medical Center, Orange, CA.
Background: Lung cancer is the most frequently diagnosed malignancy and the most common cause of cancer related mortality worldwide. Despite early diagnosis and improvements in therapy, the overall 5-year survival rate of NSCLC is 15%. NSCLC frequently expresses EGFR and this led to the development of Iressa and Tarceva, small molecule EGFR tyrosine kinase inhibitors. However, conflicting results have been reported in correlation between an objective clinical response to TKIs and EGFR testing results due to different tests being used.
Design: FISH studies for NSCLC performed at Oncotech Inc. with IHC from 11/2005 to 4/2007 were retrospectively retrieved. H&E slides were reviewed for histologic classification including adenocarcinoma (ADE), bronchioloalveolar carcinoma (BA), poorly differentiated carcinoma (PDCA), and squamous carcinoma (SQC). The IHC stains were interpreted as negative (0, 1+) and positive (2+, and 3+). FISH results were categorized as negative (disomy, low trisomy, high trisomy, and low polysomy) and positive (high polysomy and gene amplification).
Results: Five hundred and thirty-seven patients were identified. EGFR was positive by IHC in 420 (78.2%) cases and was positive by FISH in 226 (42.1%) cases. The comparison of the results from these two methods was summarized in Table 1.

EGFR expression results by IHC and comparison with FISH

	FISH Positive	FISH Negative
IHC Positive (N=420)	194 (46.2%)	226 (53.8%)
IHC Negative (N=117)	32 (27.4%)	85 (72.6%)

The histologic correlation of 537 cases was summarized in Table 2.

Distribution of Histology for IHC and FISH Studies

Histology	Cases (N=537)	Positive by IHC (N=420)	Positive by FISH (N=226)
ADE	263	191 (72.6%)	110 (41.8%)
BA	14	6 (42.9%)	3 (21.4%)
PDCA	135	101 (74.8)	57 (42.2%)
SQC	125	112 (89.6%)	56 (44.8%)

Conclusions: IHC tends to have higher positive rates for EGFR expression, particularly for squamous carcinoma. The EGFR expression correlates with EGFR gene copy number abnormalities in half of the NSCLCs. EGFR gene copy number alterations do not always correlate with EGFR expression level. Other underlying mechanisms for

EGFR regulation exist in NSCLC. The role of current EGFR testing for guiding target therapy therefore remains to be investigated.

1725 Validation of a Novel Automated Immunohistochemistry Technology Using 13 Common IHC Antibodies in Routine Surgical Pathology

A Cotrell, J Alexis, RJ Poppiti, LM Howard, L Schiffhauer, D Hicks, E Saiz, H Yaziji. Mount Sinai Medical Center, Miami Beach, FL; University of Rochester, Rochester, NY; Vitro Molecular Laboratories, Miami, FL.

Background: Several immunohistochemistry automation systems are currently employed for diagnostic applications of IHC in surgical pathology , which had drastically improved standardization of IHC assays. The main common problem is a prolonged automated run time that varies from 1.5 to 3.5 hours. A novel automated platform has recently been developed, which is based on capillary gap technology and vacuum/motion (Celerus Diagnostics, Santa Barbara, CA). This platform claims significantly shorter run time. We wished to test this hypothesis and validate our in-vitro testing of common IHC markers on this platform.

Design: Three institutions participated in this study. 168 previously diagnosed tumors were included [breast cancers (n = 131), B-cell lymphoma (n = 5), lung adenocarcinoma (n = 15), melanoma (n = 17)]. The previously validated methodology consists of two similar types of robotic reagent-dispensing systems (Autostainer, Dako, Carpenteria and Autostainer 360, Thermo Scientific, Fremont, CA). 13 diagnostic and predictive markers (HER2, Ki-67, p53, p16, S100, MART-1, tyrosinase, vimentin, Keratin AE1/AE3, Keratin 7, CD20, PAX5) were used. Tumor sections were pretreated in pressure cooker (citrate pH=6) prior to incubating with the primary antibody, followed by a two-step polymer detection (Dako, Carpenteria, CA), followed by enzyme chromogenic localization. Parallel testing on the new technology was performed using pressure cooker pretreatment (EDTA/Tris pH = 8) and employing a similar polymer detection. Slides were scored using previously established scoring criteria for each marker.

Results: Perfect (100%) correlation was observed between the two systems, showing very similar results between the two platforms. This is also true for the predictive markers (HER2, p53, Ki-67). There was no significant quantitative or intensity difference between the two platforms. The average turnaround time on the pre-existing platform is 2.5 hours, compared to 20 minutes on the new platform.

Conclusions: The Celerus Wave technology showed identical results compared to the more established, automated IHC platform using a broad range of predictive and diagnostic antibodies. This technology offers the advantage of significantly shorter turnaround time and continuous throughput.

1726 Slide Based Molecular Analysis Technique for the Work-Up of Indeterminate Atypical Pancreatic Lesions

KD Denning, TC Pereira, SD Finkelstein, YL Liu, MK Dhawan, A Kulkarni, JF Silverman. Allegheny General Hospital, Pittsburgh; RedPath Integrated Pathology Inc., Pittsburgh; Allegheny Center for Digestive Health, Pittsburgh.

Background: Fine needle aspiration cytology (FNAC) is often the initial step in the diagnosis of solid and cystic lesions of the pancreas. Occasionally, the diagnosis can be challenging when benign ductal cells show inflammatory atypia and reparative changes in the setting of pancreatitis making it difficult to separate these lesions from well differentiated adenocarcinoma (AC). Recent studies have shown that pancreatic ACs show allelic imbalance damage for a subset of mutational markers. In this study we evaluated surgical and clinical outcomes of patients with atypical FNAC to determine if molecular analysis using a slide based technique can provide additional information for a more definitive diagnosis.

Design: Slide based microdissection followed by PCR studies were performed on 26 indeterminate atypical FNA specimens of solid and cystic pancreatic lesions. Molecular studies were performed following microdissection of multiple clusters of representative atypical cells from an original FNAC slide. The FNAC and molecular diagnosis (MD) was determined to be benign (non-aggressive) or dysplastic/malignant (aggressive) for each patient based on cytology criteria and the number of molecular abnormalities. The clinical or surgical follow-up (FU) was compared to the FNAC and MD.

Results: Of the 26 patients, 3 patients lacked surgical and/or clinical FU information. Fourteen (60.9%) patients had FNAC and MD that predicted the correct FU diagnosis of a benign course. In 4 (17.2%) patients FNAC was benign, but the MD indicated a dysplastic or malignant process and the FU revealed a malignancy. In 2 (8.7%) patients, the FNAC and MD suggested a dysplastic or malignant diagnosis and the patients were found to have AC. Two (8.7%) patients had a benign FNAC and MD, but the patients were found to have AC. One (4.3%) patient had a dysplastic FNAC diagnosis, but the MD supported a benign diagnosis and the patient was found not to have cancer on FU.

Conclusions: Our results show that using the techniques of PCR molecular analysis of microdissected material from slides was helpful in the work-up of indeterminate, atypical pancreatic FNAs. In approximately 74% of the cases, FNAC with a slide based molecular analysis predicted the correct outcome which could be of value in making a more specific diagnosis and thereby help in the appropriate management of the patient.

1727 A Case Study Demonstrating the Effect of Software Connectivity and Parallel Processing on Turn around Time

SA DeVore, K Ellison, J Schmid, RJ Lalor, JP Wright. Dako North America, Carpinteria, CA.

Background: In clinical pathology laboratories there is a common misconception that a single instrument that can process the bulk of routine immunohistochemical (IHC) work is far superior in speed to a system which separates out each process to be run individually. However, in today's laboratories with the ever increasing workload and demand on turn-around-time, the ability to parallel process by enabling independence of each process is an option to optimize the workflow. By pairing these parallel processing systems with connectivity software, steps can be eliminated.

Design: Five different clinical laboratory scenarios (Laboratory 1 – 5) were defined. For each scenario a routine workload of one hundred twenty cut and baked IHC slides per day was used. Two automated slide stainers and one histotech was defined. Each of the five laboratories were set up with varying workflow solutions ranging from a single system with limited laboratory connectivity to fully integrated batch processing instruments with parallel processing and software connectivity. The five scenarios were defined as: 1: 2x 30 Slide Capacity (SC) Stainers, Single Piece Flow, no LIS/LAN Connectivity 2: 2x 48 SC Stainers, manual Deparaffinization and Antigen Retrieval, no LIS/LAN connectivity 3: 2x 48 SC Stainers, 2x PreTreatment Modules, no LIS/LAN connectivity 4: 2x 48 SC Stainers, 2x PreTreatment Modules, full LAN/LIS connectivity 5: 2x 48 SC Stainers, 2x PreTreatment Modules, full LAN/LIS connectivity Scenarios 1-4 included thirty slides per batch. Scenario 5 included forty-eight slides per batch. Time data was collected externally and in-house from the beginning of a work day until the last slide was cover slipped and ready for review (daily total processing time). Each individual process was timed and characterized into two groups: manual or automated, and total time spent was recorded.

Results: Calculating the Turn-Around-Time (TAT) for all scenarios showed that TAT for Scenario 1 produced the maximum time (Time: 10 hrs, 45 min). In Scenario 5 the TAT was reduced by 44% (Time: 6 hrs). Scenario 1 had a 30% higher Hands-on-Time compared with Scenario 5. Varying configurations of laboratory connectivity and integrated workflow solutions showed different levels for TAT between these two extremes.

Conclusions: A workflow which allows for a continuous flow and treatment of slides through parallel processing can be up to 44% faster than a single piece flow system. Adding software connectivity to the process further enhances efficiency in the laboratory.

1728 Flow Cytometric Evaluation of Reactive and Dysplastic Granulocyte Maturation by a Novel Method of High Dimensional Data Analysis

WG Finn, KM Carter, R Raich, A Harrington, SH Kroft, AO Hero. University of Michigan, Ann Arbor, MI; Oregon State University, Corvallis, OR; Medical College of Wisconsin, Milwaukee, WI.

Background: Traditional flow cytometry methods do not fully exploit the dimensionality of the data. We recently demonstrated the analysis of flow cytometry datasets as single high-dimensional objects via a novel method called FINE (Fisher information non-parametric embedding), that uses principles of information geometry and statistical manifolds to determine information distances between multidimensional datasets (Cytometry B 2008, July 18; epub ahead of print) and effectively distinguished leukemic lymphoblasts from physiologic lymphoid precursors (hematogones) in marrow. We now apply this method to the comparison of granulocyte maturation patterns in normal and dysplastic granulopoeisis, since published data are not consistent on the objective role of flow cytometry for this purpose.

Design: 28 marrow samples (11 non-neoplastic [NN] and 17 myelodysplastic [MDS]) were evaluated with a standard 4-color (6-parameter) tube measuring forward scatter (FS), side scatter (SS), CD11b, CD16, CD45, and CD56. Non-blastic granulocytes/precursors were selected by CD45 vs SS, and listmode datasets were analyzed by FINE, which 1)converts the 6-parameter listmode data in each case into 6-dimensional probability density functions via a kernel density estimate, 2)compares information distances via an entropy measurement, the Kullback-Liebler (K-L) divergence, and 3)constructs high-dimensional neighborhood maps of K-L divergence among cases, projecting these maps onto 2-dimensional (2D) plots for visual comparison.

Results: 10 MDS cases (4 RAEB, 3 RCMD, 3 MDS unclassified) formed a discrete cluster in FINE space. 7 MDS cases (2 RARS, 3 RCMD, 2 MDS unclassified) showed some overlap with the NN samples. One NN sample (maturation arrest due to early recovery from drug induced agranulocytosis) embedded within the MDS cluster.

Conclusions: Our analysis effectively separated high-grade MDS (all RAEB and half of RCMD cases) from NN marrow samples, but showed some overlap between NN and MDS overall. These data provide a demonstration of principle that granulocyte maturation patterns may be objectively compared by an algorithm (FINE) that treats flow cytometry data as single high-dimensional objects rather than as a series of 2D histograms. The clustering of a case of regenerative maturation arrest with MDS cases warrants additional study of similar cases.

1729 Spiral TMA, a Novel Technique To Make TMAs without Coring Tissue

J Fukuoka, T Uemura, T Tanaka, MD Hofer, S Kageyama, T Hori. Toyama University Hospital, Toyama, Japan; Brigham and Women's Hospital, Boston, MA.

Background: Tissue microarrays (TMAs) are an established technique to bridge basic science research and clinical use allowing to determine the clinical significance of molecules. Yet, at the same time, conventional TMAs have several limitations such as tissue heterogeneity and frequent core loss due to uneven thickness of the donor block. To solve these problems, we developed a method, Spiral TMA (s-TMA). Here, we describe construction of spiral TMAs and demonstrate the concurrence of immunohistochemical staining results between s-TMA and conventional pathology specimens using the same blocks.

Design: For s-TMA, tissue is not cored from the donor block but thick slices of donor tissues reeled and arrayed as tissue cylinders. Major advantages are that tissue heterogeneity is represented, that TMAs from blocks with thin tissues layers can be constructed, the tissue loss from TMA slides due to the difference of tissue thickness is minimized and that the morphology of the array slide is visible before staining. Six cases were selected from case archives of Toyama University Hospital and 50 um thick specimens were cut from each case. Specimens were reeled and sectioned into cylinders 4 mm tall and arrayed in a recipient block with 3mm holes to form a s-TMA block.

Five um thick specimens were cut from both TMA and original blocks and stained for Ki-67 which was evaluated by counting maximum and minimum percentage of positive cells at 40x.

Results: As listed in the table, Ki-67 staining was concurrent between s-TMA and conventional sections with agreement in maximum staining percentage between 100 – 35.5 % (median rate concurrence: 91.7%).

Table: Ki-67 in s-TMA and conventional slides.

Table 1	Spiral TMA		Conventional tissue	
Sample(organ)	Max	Min	Max	Min
Core1 (lung)	57.1(%)	27.6(%)	66.1(%)	5.6(%)
Core2 (ovary)	81.1	23.4	89.3	1.2
Core3 (ovary)	78.6	23.4	83.0	8.7
Core4 (panc)	75.5	25.4	81.6	6.4
Core5 (rectum)	96.1	39.6	82.6	28.9
Core6 (kidney)	5.3	1.6	14.7	1.5

Conclusions: We introduce a newly developed technique, spiral TMA, that resolves some of the limitations encountered with convential TMAs. We validated its quality and accuracy of tissue representation. Our results further indicate that spiral TMA covers increased tissue heterogeneity, one of the major criticisms of conventional TMAs.

1730 Using Histogram Image Analysis To Improve the Interpretation of Ac-Histone H3 Biomarker Expression in HDAC Inhibitor Treated Xenograft

Y Gao, R Mosher, J Deeds. Novartis Institutes for BioMedical Research, Inc., Cambridge, MA.

Background: Acetylated-histone H3 (Ac-H3) increases with HDAC inhibition. Ac-H3 was examined in treated xenograft models. In initial studies, thresholds to determine levels of Ac-H3 were set empirically with binned values. The purpose of this study was to determine if additional information could be obtained by looking at this IHC data as a continuous series, rather than discrete values.

Design: The Ac-H3 antibody was evaluated on tissue sections from three animals treated with 20 mg/kg of an HDAC inhibitor over a series of dilutions using the Ventana Immunostainer. Whole tissue images were analyzed using the Aperio Scanscope and the Aperio Imagescope IHC Nuclear Algorithm Version 8.0 software. First, the slides were examined by setting manual thresholds for positive signal. The slides were re-examined using a histogram representation of all the data points, to see if additional information could be revealed.

Results: By eye, a greater difference could be seen between groups as the antibody was titrated. At a titration of 1:1000, we could easily set an empirical threshold for staining that allowed us to bin samples into treated vs untreated. When frequency data was plotted for all optical density values, and ROC curves generated, we could see that the "by eye" threshold favored specificity over sensitivity. Furthermore, while the higher concentration assays were difficult to interpret by eye, the higher antibody concentration caused the ROC curve to shift to the upper left hand corner.

Conclusions: 1) Empirical interpretation can be improved by examining a series of titrations. 2) Empirical threshold can be examined against ROC curves to understand the relative value of sensitivity and specificity. 3) Image analysis methods may perform best at titrations that are not optimal for empirical reads.

1731 Use of Multispectral Microscopy To Distinguish Reactive Urothelium from Neoplastic

CM Gilbert, AV Parwani. University of Pittsburgh Medical Center, Pittsburgh, PA.

Background: The interpretation of urothelial atypia in a setting of chronic inflammation and reactive changes can prove quite difficult. Ancillary studies such as CK20, P53, and CD44 have been shown to be of great value in these instances. The aim of this study is to evaluate a triple-immunostain with the assistance of multi-spectral microscopy in order to, in a single slide, evaluate their simultaneous expression and location in urothelium, and, at the same time, diminish the risk of loosing the area of interest in further recut sections.

Design: 53 bladder biopsies with previous diagnosis of benign/reactive, dysplastic, carcinoma in situ or carcinoma (approximately 39 cases spanning 1998-2006) were prepared using a triple-immunostain cocktail consisting of CK20, P53 and CD44. Three control stains were used for the purpose of creating a spectral library for the Nuance CRI Flex microscopy system (spectral range of 420 to 720 nm). The bright-field mode was used for analysis. All specimens were captured and analyzed with the custom built spectral template and analyzed using the provided Nuance software version 2.71. CK20 was given a score of 1 if it involved the upper 1/3, 2 for 2/3, and 3 for full thickness staining. P53 was scored as 0 (neg), 1+ (weak), 2+ (moderate) and 3+ (heavy). CD44 was not scored as it proved difficult to interpret in many cases.

Results: The results demonstrated that it was possible to separate the multiple stains co-localized in the biopsies, including the counterstains. Separation of the stains demonstrated a correlation of p53 and CK20 dual expression in biopsies diagnosed as carcinoma. Low or undetectable levels of expression were seen in biopsies later diagnosed as reactive or benign. Using this method, for benign or reactive cases, CK20 was restricted to the upper 1/3 in 17/23 biopsies (74%) and p53 was weak or negative in 11/23 biopsies (55%). No benign or reactive biopsies stained heavily (3+) for p53. For cases of carcinoma in situ or invasive disease CK20 was expressed in the upper 2/3 or full thickness in 19/26 (73%) and p53 was moderate or heavy in 19/26 cases (73%). Dysplastic biopsies appeared to resemble benign reactive biopsies with only 2/6 (30%) expressing moderate or heavy p53 and CK20 restricted to the upper 1/3 in 66% (4/6) of the biopsies.

Conclusions: The combination of multispectral microscopy and multiple immunostain "cocktails" form a powerful and useful tool for the interpretation of small biopsies with faint or difficult to interpret staining and for cases with limited material such as small needle core biopsies.

1732 Remote Real Time Reporting of Urgent Liver Biopsies: Whole Slide Imaging Is Feasible in a Quaternary Care Academic Center

M Guindi, SL Asa, AJ Evans, R Chetty. University Health Network, Toronto, ON, Canada.

Background: The acquisition of Telepathology (TP) systems in North America is steadily increasing along with interest in its diagnostic uses. At University Health Network (UHN), whole-slide imaging (WSI) which represents a major technological advance in the area of TP, is available routinely. UHN is a large liver referral center in Canada with one of the largest liver transplant programs in North America. Thus, there is a constant need for urgent liver biopsy (LB) interpretation especially post-transplant biopsies requiring subspecialty expertise. **Objectives:** To test the feasibility and diagnostic accuracy of utilization of WSI for the off site reporting of urgent LB in real time.

Design: From February 2008 to September 2008, off hours (after 5pm) urgent LB were interpreted by TP using WSI. H and E sections (+/- trichrome) were scanned at 20x by histotechnologists to create compressed JPEG files. Patient identifiers were removed, and files uploaded via a UHN portal creating an internet link that is emailed to the off site pathologist, who accessed the scanned slides via the UHN email system, viewed them on their computer or laptop, and communicated the diagnosis directly to the UHN hepatologist or surgeon by email or phone. The glass slides were later evaluated by light microscopy (LM) and, TP and LM diagnoses compared. A survey of 15 clinicians (hepatologists and surgeons) receiving this service was also conducted. service was conducted.

Results: WSI was used to make 22 primary LB diagnoses. Out of hospital sites of reporting included pathologist's residence, Denver at USCAP 2008, San Diego, and Montreal. Case mix: 15 post transplant LB? rejection, 3 donor LB, 2 nontransplant LB, 2 liver failure LB (1 at pretransplant work up). Download time of files: mean 7.25 and median 1.57 minutes. An average of 10 minutes was required to review WSI file(s) for a diagnosis. File size: mean 56 and median 41 Mbytes/slide (range 22.5-143). Diagnostic accuracy was 99% for WSI compared to LM. In 2 cases, only preliminary diagnoses could be made by TP and LM; final diagnosis required the aid of immunohistochemical stains.

Conclusions: TP allows continuity of subspecialty interpretation of urgent LB while the pathologist is out of town, readily facilitates consultation with non-liver pathologist colleagues on call thus improving on call services, and has been met with unanimous acceptance and admiration of user clinicians. Diagnostic accuracy and timeliness is unaffected by the use of TP.

1733 Detection of Cervical Intraepithelial Neoplasia (CIN) by Spectral Similarity Mapping Histology and Computer-Assisted Classification

AON Joseph, G Galliano, S Bose, DL Farkas. Cedars Sinai Medical Center, LA, CA; Cedars Sinai Medical Center, LA, CA.

Background: Screening for cervical carcinoma and its precursors by standard cervical pathology has known problems. There is a need for new methods for better detection and discrimination of CIN. Using new optics and/or automated image analysis to reduce subjectivity should provide effective screening tools for early detection of cervical cancer. However, long-term studies using available cervical images are needed to validate the potential of new algorithms in discriminating CIN from normal tissue.

Design: This clinical study examined the diagnostic potential of spectral imaging and automated image processing in patients with CIN with the extreme grades of negative and CIN III. We investigated the use of spectral imaging - based on combining spectroscopy and digital imaging - for analysis of dyes and enzyme precipitates on pathological specimens. A pixel-by-pixel spectrum-based color classification of single and double color immunocytochemical staining of H&E in paraffin-embedded cervical tissue samples was performed. Ten stage CIN III, and 5 negative patients were sampled for a total of 53 image sets. Images were collected from 450-800 nm for data cubes consisting of 46 wavelengths. All slides were imaged by using a Zeiss microscope and our modified commercial spectral instrument, at 10X objective magnification, yielding up to 700 MB of uncompressed data per set. Established spectral unmixing techniques separated regions of interest and quantified presence of indicators. The cases were also examined and marked by two experienced pathologists.

Results: The results demonstrate that spectral imaging can reliably identify chromogenic dyes in a single bright-field microscopic specimen. Regions of interest (ROI) were segmented, quantified, and used to build a spectral reference database of disease. Separate microscopic fields from the same patient can be analyzed using this spectral reference library, to check reproducibility.

Conclusions: We conclude that spectral imaging is a reliable and robust method for pixel color recognition and classification in CIN. Our data further indicate that the use of spectral imaging a. can increase the number of parameters studied simultaneously in pathological diagnosis, b. may provide quantitative data (such as positive labeling indices) more accurately, c. may solve segmentation problems currently faced in automated screening of tissue specimens and d. can enhance the objectivity and reproducibility of histopathologic diagnosis.

1734 The Isoelectric Point (pI) of Epitope May Be the One of the Determinant Factor for the Effective Heat-Induced Epitope Retrieval

H Kajiya, S Takekoshi, M Takei, RY Osamura. Tokai University School of Medicine, Isehara, Kanagawa, Japan; Nippon Medical School, Sendagi, Tokyo, Japan.

Background: The localization of nuclear proteins has been benefitted by heat induced epitope retrieval(HIER). This technical study is aimed at to elucidate the relationship between the pH of retrieval buffer used in HIER and the isoelectric point (pI) of epitopes for various antibodies against human pituitary transcription factors, i.e. NeuroD1, TBX19, GATA2, DAX1, PROP1, PITX1, MSX1, in order to clarify the background mechanisms in HIER method for the particular antibodies using FFPE pituitary adenomas.

Design: Tissues of pituitary adenomas were obtained by surgery and immediately formalin-fixed and paraffin-embedded(FFPE). Deparaffinized sections were treated for HIER method (autoclave heating; 121C, 5min) using universal buffer (Teorell-Stenhagen citrate-phosphate-borate buffer), which has a buffering capacity over a wide range pH from 2.0 to 12.0. For immunostainig, biotin avidin peroxidase complex (ABC) method was used.The pI of each transcription factor and corresponding adenomas cases are summarized in the Table.

Results: In our study, all pituitary transcription factors were strongly immunostained in the nuclei after HIER in universal buffer, simply depending on buffer pH value.

pH-dependent antigen retrieval for human pituitary transcription factors

Antigens	Pituitary adenoma	pI	Non heating	pH 3.0	pH 6.0	pH 9.0
Neuro D1	ACTHoma	4.53	-	-	-	+
Ptx1	GHoma	4.83	-	+/-	-	+++
GATA2	TSHoma	7.40	-	+++	+/-	++
DAX1	Non functioning	8.49	-	+++	+	++
TBX19	ACTHoma	9.31	-	++	-	+/-
Prop1	GHoma	12.70	-	+++	-	+/-

immunostaining was scored as follows: +++, strong; ++, moderate; +, weak; ± faint; -, negative

It should be particularly emphasized that, in order to give the most appropriate staining by the efficient HIER, antigen epitopes with acidic pI(negatively charged) required basic pH buffer conditions, while antigen epitopes with alkaline pI(positively charged) required acidic pH buffer conditions, This suggests that electrostatic charges of epitopes are essential to achieve the best results by HIER for individual antibodies.

Conclusions: From our studies, it should be pointed out that the pH of the buffer and pI of the epitopes are of great importance for electrostatic charges of the individual transcription factors for retrieval. The pI of epitopes may be the one of the determinant factor for the mechanism of HIER to achieve the best results on immunohistochemical staining.

1735 Comparison of Desmoplastic Reaction and Invading Ability in Invasive Ductal Carcinoma (IDC) of Breast and Prostatic Adenocarcinoma Based on Expressions of Hsp47 and Fascin

AR Kandiloglu, N Nese, G Simsek, M Lekili, A Ozdamar, A Catalkaya, T Coskun. Celal Bayar University, Manisa, Turkey.

Background: IDC is characterized by prominent desmoplasia, whereas conventional PCa generally have little/no desmoplastic reaction. HSP47 is major collagen specific chaperone responsible for formation and maturation of collagen during protein synthesis. Fascin, an actin binding protein, plays important role in cancer invasion and metastasis. Both these proteins are overexpressed by various carcinomas. We investigated the diversity within IDC and PCa by evaluating immunohistochemical expressions of HSP47 and fascin, the molecules which are related to desmoplasia and invasion, and analyzed its correlation with clinicopathological parameters.

Design: Forty nine mastectomies and 57 radical prostatectomies were immunostained with HSP47 and fascin. 10 mammoplasty specimens and 10 prostatectomy specimens performed for prostate hyperplasia were chosen as control group. Immunoreactivity (IR) was evaluated as: 0: <5%, 1+: 5-25%, 2+: 25-50%, 3+: >50%. Desmoplasia was designated as 0 to 3.

Results: HSP47 and fascin were localized to cytoplasm and were significantly more often expressed in both the tumors than control groups ($p<0.05$). PCa demonstrated immunoreactivity to HSP47 significantly more often than IDC. Tumor size correlated with fascin expression in IDC ($p<0.05$). HSP47 expression was noted significantly more often in PCa involving both left and right lobes.

Clinicopathologic Parameters and Immunohistochemical Evaluation

IDC		PCa	
Mean age	55 years		67 years
Mean tumor size	3.3 cm	Mean PSA level	12.7 ngr/dl
Poorly-differantiated tumor	12.2%	Gleason score 8-10	19.3%
c-erbB-2 (2+/3+) score	33%	Extraprostatic extension	29.8%
ER negativity	26.5%	Seminal vesicle involvement	15.8%
PR negativity	32.7%	Involvement of both right and left lobes	88%
Axillary LN positivity	69%	Recurrence	11.6%
Mean follow-up	42 months (64%)		52 months (75%)
Metastasis	13.3%		9.3%
Dead of disease	20.0%		4.7%
Desmoplasia	100%		11%
HSP47 (2+ and 3+ IR)	29%		42%
HSP47 in control cases (n=10)	0%		20%
Fascin (2+ and 3+ IR)	65%		23%
Fascin in control cases (n=10)	0%		0%

Conclusions: HSP47 and fascin expression may play role in the pathogenesis of IDC and PCa because their expression is significantly higher in IDC and PCa than their normal counterpart. Although there is no relationship with recurrence or metastatic status, fascin overexpression correlated with tumor size which may prompt its use as a prognostic factor in IDC.

1736 Diagnostic Utility of Trichrome Stain for the Evaluation of Amyloid Deposition in Tissue Sections

J Karamchandani, JD Faix, G Berry, A Sangoi. Stanford University Medical Center, Stanford, CA.

Background: Amyloid is customarily identified by "apple-green" birefringence under polarized light, though the use of Congo red staining for amyloid detection in routine surgical pathology can be fraught with difficulty as the degree of alcohol differentiation can affect sensitivity. In an informal setting, we have characterized a unique pattern of amyloid staining when viewed with trichrome stain. Given this finding, a formal comparison of the amyloid staining properties of Congo red and trichrome was performed, results which have not previously been reported.

Design: Trichrome and Congo red stains were performed on formalin-fixed paraffin embedded blocks from 10 cases. Trichrome stains employed DAKO's Gomori's Trichrome Kit with an Artisan automated slide stainer. Where possible, thioflavin S staining or electron microscopy was performed to further confirm amyloid deposition. Staining intensity was semiquantitatively scored as 0 to 3.

Results: Amyloid appears grayish-blue on trichrome stained section by light microscopy (LM), and has a consistently distinct appearance from that of collagen (dark blue). The presence of amyloid was further established with either Thioflavin S (viewed with UV light) or electron microscopy. In 5/10 cases, trichrome stain suggested greater presence of amyloid than Congo red. Staining intensity by organ is listed in Table 1.

Table 1

Organ	**Diagnosis**	Trichrome (LM)	Congo Red (polarized)	Additional Studies
Heart	Cardiac amyloidosis	3	1	EM
Liver	Hepatic amyloidosis	3	1	T-S
Pituitary	Prolactin-secreting adenoma	3	1	T-S
Skin	Systemic amyloidosis	3	1	T-S
Skin	Nodular amyloidosis	3	2	T-S
Duodenum	Intestinal amyloidosis	3	3	N/A
Prostate	Seminal vesicle amyloidosis	3	3	N/A
Soft tissue (abdomen)	Amyloidosis	3	3	T-S
Thyroid	Medullary Carcinoma	3	3	N/A
Vocal Cord	Amyloidosis	3	3	T-S

EM=electron microscopy, T-S=thioflavin S, N/A=not available

Conclusions: While Thioflavin S staining examined under UV light and/or ultrastructural analysis are highly sensitive and specific for amyloid detection, Congo red stain is routinely employed in surgical pathology to detect amyloid. Congo red requires procedural proficiency for reliable diagnostic utility, as nonspecific and false negative staining can occur. Trichrome's unique tinctorial staining pattern may highlight more amyloid than is detected with routine Congo red staining when viewed with polarization. Trichrome's low procedural complexity, tinctorial reproducibility, and use with LM further advocate its use as an adjunct stain for diagnostic amyloid detection.

1737 Detection of microRNAs in Frozen Peripheral Blood Samples from Patients with Chronic Lymphocytic Leukemia

P Kaur, CL Bartels, GJ Tsongalis. Dartmouth Medical School, Dartmouth Hitchcock Medical Center, and Norris Cotton Cancer Center, Lebanon, NH.

Background: Chronic lymphocytic leukemia (CLL) is the most common leukemia in the western world. Recently research, conducted primarily in basic science laboratories, has indicated a role for microRNAs (miRNAs) in the pathogenesis and prognosis of this disease. MiRNAs are a family of endogenous, small, non-coding, functional RNAs. They mediate post-transcriptional inhibition of messenger RNAs, and hence can function as tumor suppressors or oncogenes depending on their target genes. Here we demonstrate that miRNA expression levels in CLL patient samples can be determined retrospectively using archived frozen peripheral blood samples.

Design: In the present study, RNA samples from sixteen CLL patients were obtained from snap-frozen residual flow cytometry (peripheral blood) specimens. Samples were collected between 2004 and 2007 and stored at -80°C. Total RNA was extracted from WBCs using the *mir*Vana™ miRNA Isolation Kit (Ambion) and expression of miR15a, miR16-1, miR29a, miR181a, and U47 (an endogenous control) in each sample was determined using TaqMan® MicroRNA Assays (Applied Biosytems). In addition, expression of these miRNAs was determined in white blood cells from five normal samples. The DCt of the normal (Ct_{normal} - $Ct_{endogenous\ control}$) and CLL samples ($Ct_{CLL\ sample}$ - $Ct_{endogneous\ control}$) were calculated, and relative comparison of normal and CLL samples was made using the DDCt method (DCt_{normal} - $DCt_{CLL\ sample}$).

Results: We found that expression miR15a and miR16-1 is reduced in CLL patients compared to normal samples (Figure 1). Two other miRNAs, miR29a and miR181a showed variable expression. miR29a showed an increase in expression in most of these cases, while miR181a was decreased in all but 2 cases

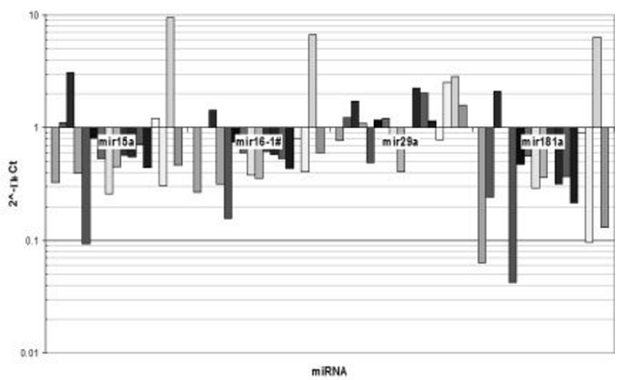

Figure 1. Expression of select microRNAs in frozen peripheral blood samples of CLL patients.

Conclusions: Our study indicates that the TaqMan® MicroRNA Assays are suitable for determining miRNA expression levels in CLL patients. In addition, these real-time PCR assays can be performed on archived frozen aliquots of whole blood.

1738 Determining the Recovery Efficiency and Relative Enrichment of Circulating Tumor Cells Using the CellSearch System in Patients with Metastatic Lung Cancer

DW Kindelberger, LM Flores, ES Cibas, AH Ligon, MF Loda, IE Krop, PA Janne. Brigham and Women's Hospital, Boston, MA; Dana-Farber Cancer Institute, Boston, MA.

Background: Circulating tumor cells (CTCs) in the peripheral blood of patients with metastatic cancers have been increasingly accepted as indicators of prognosis and treatment response. Applications for purified CTCs, including fluorescence *in situ* hybridization (FISH) and direct sequencing, continue to increase. The CellSearch platform (Veridex, LLC), begins with a tube of peripheral blood and generates a sample enriched for CTCs. The CTCs can be either processed for counting or left uncounted for downstream applications. This study characterized both "counted" and "uncounted" samples, using H&E staining, immunohistochemistry (IHC), and FISH to evaluate the absolute number of CTCs and their relative enrichment.

Design: Peripheral blood samples were collected from 21 patients with biopsy-confirmed metastatic lung adenocarcinoma (three 7.5 ml tubes/patient). One tube was processed for counting and the remaining two tubes were processed uncounted for FISH and IHC, according to CellSearch protocols. Following enumeration of the counted samples with the CellTracks system, the cells were washed, fixed, and processed as cytospin slides followed by H&E staining. Uncounted samples were similarly washed, fixed, and processed as cytospin slides, followed by either H&E staining, IHC (using AE1/AE3), or FISH using probes against CEP7, EGFR, and MET. Cell numbers were determined by manually counting H&E-stained and FISH slides. CTCs were identified by AE1/AE3 IHC if they demonstrated circumferential membrane staining. CTCs were identified by FISH as those cells having greater than 2 signals with the CEP7 and/or EGFR/MET probes.

Results: For all cases, the number of tumor cells determined by H&E staining (mean 10.5) was significantly greater than the number determined by the CellTracks system enumeration (mean 1.8). Additionally, in all cases, the number of cells in counted samples was less than that seen in corresponding uncounted samples. The AE1/AE3 IHC and FISH results were concordant and showed that CTCs made up over 50% of the isolated cells.

Conclusions: Samples processed using the CellSearch system are significantly enriched for tumor cells. The CellTracks enumeration system appears to underestimate the true number of circulating tumor cells. "Uncounted" samples are sufficiently enriched for CTCs to allow for numerous downstream applications such as FISH and direct sequencing.

1739 Development of Methods for Loss of Heterozygosity Studies When Normal Specimens Are Not Available

JA Lefferts, GV Belanger, CT Spyris, JB Brennick, AR Schned, GJ Tsongalis. Dartmouth-Hitchcock Medical Center, Lebanon, NH; Dartmouth Medical School/Dartmouth College, Hanover, NH; Norris Cotton Cancer Center, Lebanon, NH.

Background: Loss of heterozygosity (LOH) is often performed retrospectively and is often hindered by the lack of readily available normal tissue or blood specimens from which a reference DNA sample can be extracted. Microsatellite markers having numerous alleles of varying lengths are typically amplified by PCR from both tumor and normal DNA. Complete loss of one allele peak or significant changes in relative peak heights in the tumor sample can be classified as exhibiting LOH. We have examined a novel method for determining LOH in the absence of matched, normal DNA samples.

Design: Microsatellite (STR) sequences were PCR amplified from normal de-identified human genomic DNA samples and subjected to capillary electrophoresis. Peak height ratios (longer peak height/shorter peak height) were calculated for all samples found to be heterozygous with respect to each STR. The heterozygous peak height ratios were then plotted against the differences in length between the two observed alleles to create standard curves of expected ratios. For each point on the standard curve, a statistical range of expected ratios was calculated. Results from prior LOH studies based on DNA extracted from six renal carcinomas of various sub-types, seven basal cell carcinomas and three squamous cell carcinomas were then applied to these standard curves.

Results: Linear relationships were observed for each STR evaluated with R squared values as high as 0.96 when the peak height ratios for each sample were compared to differences in allele lengths. Peak height ratios of cancer specimens from previous LOH studies were applied to these standard curves. A strong correlation was found between the LOH status of samples as determined using the standard curves and the LOH status of the same samples as determined previously.

Conclusions: 1) A linear relationship exists between peak height ratios of alleles in normal heterozygous DNA and the difference in length of the two alleles 2) This relationship can be utilized to predict the expected range of peak height ratios of two alleles in normal DNA samples that exhibit a specific difference in length. 3) Tumor samples with peak height ratios outside the expected range could be considered to exhibit LOH in the absence of normal DNA samples.

1740 KRAS Mutation Detection by a PCR-Based TaqMan Assay Compared to Traditional DNA Sequencing

JA Lefferts, HA Bentley, D Le Corre, P Laurent-Puig, M Gupta, AA Suriawinata, GJ Tsongalis. Dartmouth-Hitchcock Medical Center, Lebanon, NH; Dartmouth Medical School, Hanover, NH; INSERM, Paris, France; Universite Paris Descartes, Paris, France; Hopital Europeen Georges Pompidou, Paris, France; Norris Cotton Cancer Center, Lebanon, NH.

Background: Clinical interest has been growing in tests that accurately determine the presence or absence of somatic mutations in the KRAS gene, mainly those found in codons 12 and 13. KRAS mutations have been identified in several cancer types and the presence of these mutations has been shown to indicate poorer prognoses. Many molecular diagnostic laboratories do not currently have DNA sequencing capabilities need for KRAS mutation detection. Additionally, due to the extensive manipulation required of PCR amplified DNA, extreme measures must be taken to avoid PCR contamination which can result in false-postive results. Alternative methods of mutation detection for KRAS have been developed but still tend to be time consuming and do not decrease the possibility PCR contamination. Here, we evaluate a new method of KRAS mutation detection which uses real-time PCR, producing faster results and eliminating the need for post-PCR manipulation.

Design: Twenty-five DNA samples extracted from FFPE sections of resected adenocarcinomas of the colon and seven from mucinous ovarian tumors, which had previously been subjected to KRAS DNA sequencing, were used in a TaqMan real-time PCR assay. For each sample a set of seven primer/probe mixes, each designed to detect one of the seven point mutations commonly seen in KRAS, were used to detect wild-type and/or mutant alleles.

Results: Both DNA sequencing and the TaqMan assay detected codon 12 or 13 mutations in the same ten DNA samples. The remaining 22 samples were found to be negative for KRAS mutations by both methods. Mutations in synthetic and cell line-derived DNA positive controls were also recognized by the TaqMan assay. One primer/probe set which had been designed to detect the G12C mutation was found to correctly identify known G12C sequencing but was also observed to detect other codon 12 mutations.

Conclusions: Real-time PCR using TaqMan probes to determine mutational status of KRAS in tumor specimens is a viable alternative to traditional sequencing. This assay provides results similar to those obtained by sequencing in less time without handling of PCR-amplified DNA and only requires real-time PCR instruments normally found in molecular diagnostic laboratories.

1741 The Role of Imaging-Guided Pelvic or Retroperitoneal Biopsies in Patients with Suspected Gyencological Neoplasms

A Malpica, ED Euscher. The University of Texas M.D. Anderson Cancer Center, Houston, TX.

Background: Imaging-guided pelvic or retroperitoneal biopsies (bxs) have become a tool in the work-up of patients with a suspected gynecological neoplasm. We present our experience with 37 cases of suspected gynecological tumors that underwent an imaging-guided pelvic or retroperitoneal bx as part of their work-up.

Design: In a period of 36 mos 65 women underwent a pelvic or retroperitoneal mass CT-, MRI- or ultrasound-guided bx as part of their work-up. 37 of them were suspected to have a gynecological neoplasm. The pathology reports and medical charts of all these cases were reviewed. The following information was recorded: indication for the procedure, bx diagnosis (dx), cytology material dx, dx on subsquent bx/surgical procedure if performed.

Results: Indications for the procedure included: initial dx of a neoplasm (8 cases), dx of recurrent neoplasm (21 cases), distinction between a non-gynecological primary versus a gynecological primary (5 cases), assessment of extension of disease (2 cases) and verification of tumor type (1 case). In 31 the imaging-guided bx provided tissue for histologic and cytologic evaluation. In 6 cases only tissue for histologic examination was obtained. The initial dx was provided in 6 cases while the dx of recurrent tumor was provided in 16 cases. In 2 cases, the dxs of non-neoplastic conditions were rendered: 1 abscess and 1 fibrosis post-radiotherapy. In 4 cases, non-gynecological primaries were diagnosed: 2 metastatic breast carcinomas, 1 metastatic gastric carcinoma and 1 metastatic lung carcinoma. In 19% (7/37) of the cases the results of the histology and cytology evaluations were discrepant as follows: bx with tumor and cytology material non-diagnostic, 3 cases; bx with no tumor and cytology material with tumor, 2 cases; bx with fibrous tissue consistent with radiotherapy-induced changes and cytology material non-diagnostic , 1 cas; discrepant tumor dx between histology and cytology material, 1 case (mesothelioma dx on the biopsy and adenocarcinoma on cytology material). In 22% (8/37) of the cases the material obtained by the image-guided bx was considered insufficient for dx.

Conclusions: Image-guided pelvic or retroperitoneal bxs represent a useful tool in the work-up of patients with suspected gynecological neoplasms.The procurement of both histology and cytology material increases the chances of rendering an accurate dxs. Attending physicians need to be aware that dx discrepancies can exist and these can be related to sampling artifact or error in interpretation.

1742 Standardization of Gross Room Procedures Using High-Definition Video Recordings for Improving Residency Training and Patient Safety

DS McClintock, JB Bakst. University of Chicago Medical Center, Chicago, IL.

Background: Gross examination of surgical pathology specimens is often an overlooked yet extremely important step in surgical pathology workflow as it generates the diagnostic materials upon which future patient management may be based. While written procedure manuals exist and are mandated by CAP to supplement the gross examination process, experience has shown actual use of these manuals is often short-lived given the environment and nature of the work involved. Underuse or failure to adhere to standardized grossing procedures can result in delays in diagnosis, incur extra operating costs, and in the worst case scenario, lead to errors, misdiagnosis, and poor patient outcomes. To address these issues, we have developed a method of standardizing resident training in the gross room using high-definition (HD) video recordings of gross specimen triaging and dissections.

Design: The goal of this project was to create high quality digital videos to be used as decision support aids in the real-time workflow of the gross room. An HD video recorder (Sony HDR-SR12) was used to create short instructional videos detailing grossing procedures. Audio narrations were created separately and added during the editing process, with completed videos made available online and accessible to computers at the grossing stations.

Results: Pilot videos were created for two organ systems (Figure 1). For each organ system the videos show in great clarity each step involved in the grossing process, including the initial triaging (weights, measurements, inking, opening), dissection, and cutting. The videos were introduced into the normal workflow of the gross room as a trial during resident training and for senior residents returning to their surgical pathology rotations.

Figure 1 - Videos created for specific organ systems

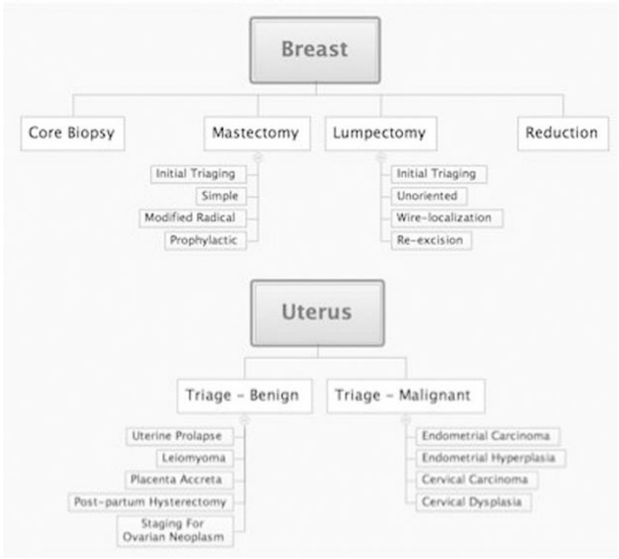

Conclusions: The use of HD instructional videos within the regular grossing workflow has the potential to reduce triaging and grossing errors amongst both new trainees and experienced pathology residents. These high quality videos can be made as specimens become progressively available; following production they can be viewed via computers at the grossing stations, providing real-time decision support while standardizing the gross examination experience.

1743 Automated Cellular Imaging System for Assessing HER-2 Status in Breast Cancer Specimens

DM Minot, BR Kipp, RM Root, A Nassar, AC Clayton. Mayo Clinic, Rochester, MN.

Background: Previous studies suggest that automated immunohistochemistry (IHC) may improve the accuracy and reproducibility of HER2 IHC testing. The goal of this study was to assess the performance characteristics of the Automated Cellular Imaging System III (ACIS) for HER2 analysis using three scoring methodologies and comparing these results to both manual pathology interpretation and FISH analysis for HER2 amplification.

Design: This retrospective study was performed on 159 biopsy slides from patients who underwent routine HER2 testing between January and February, 2008. The three ACIS scoring methods included the Equal Distribution Score (EQD), Hot Spots Only (HSO), and Ten Region Score (TRS). The HSO method consisted of selecting six areas that appeared (by visual examination of the digitalized image) to have the most intense staining. The EQD method consisted of collecting six areas including 2 areas of high, 2 areas of moderate, and 2 areas of low intensity staining. The TRS method consisted of collecting 10 areas that the operator thought would give the best overall average intensity of the entire specimen. FISH for HER2 amplification was performed using the PathVysion™ HER2 DNA probe kit.

Results: The number of IHC 0 or 1+/FISH positive cases was equivalent for all methods studied, yet the EQD and TRS method had significantly ($P<0.001$) fewer 2+ cases (n=16) and (n=18) respectively, versus the manual method (n=35). Both methods, EQD and TRS, had higher positive predictive values (PPV) (38%) and (33%) respectively, versus the manual method (20%). The percentage of patients with a (+) FISH result based on IHC scores is summarized in Table 1.

Percentage of Patients with a Positive FISH Result Based on IHC Scores

	0	1+	2+	3+
Pathologist Manual Interpretation	0/31 (0)	2/84 (2)	7/35 (20)	8/9 (89)
ACIS HSO Method	0/41 (0)	2/69 (3)	4/34 (12)	11/15 (73)
ACIS EQD Method	0/54 (0)	2/80 (3)	6/16 (38)	9/9 (100)
ACIS TRS Method	0/78 (0)	2/54 (4)	8/18 (33)	9/9 (100)

Conclusions: Both EQD and TRS methods had equivalent PPV's for the detection of FISH (+) HER2 cases and had fewer equivocal (2+) specimens, that require FISH analysis. The EQD and TRS methods may more accurately identify FISH amplified HER2 cases with fewer 2+ cases that would be reflexed to FISH analysis, when compared to the manual method. Future prospective studies are needed to determine if the ACIS can decrease the overall costs for patients undergoing HER2 testing while maintaining accurate test results.

1744 Comparison of Synthetic, Biotinylated DNA, LNA and PNA Probes for *In Situ* Hybridization (ISH) Using a Pan-Fungal rRNA Sequence: A Multispectral Imaging Study

KT Montone, MD Feldman. University of Pennsylvania, Philadelphia, PA.

Background: ISH for rRNA using DNA oligonucleotide probes can speciate fungal organisms in tissues. Locked nucleic acid (LNA) and peptide nucleic acid (PNA) probes canalso be used for rRNA ISH. LNA are modified RNA nucleotides that exhibit increased thermal stability. PNA is an artificially constructed nucleotide similar to DNA and RNA with stronger binding chanracteristics. A comparsion of these three probe types using multispectral image (MSI) analysis is undertaken in this study.

Design: 7 tissue samples with filamentous fungi were used. DNA, LNA and PNA probes targeting a pan-fungal rRNA sequence were commercially synthesized and 3' biotin-labeled. All probes were utilized at a final concentration of 1 ug/ml. ISH was performed using modified capillary action technology. Tissues were dewaxed, rehydrated and digested with pepsin. Hybridization was for 1 hour at 37ºC for DNA and 50ºC for LNA/PNA probes. Tissues were washed with either 2XSSC (low stringency) or 0.5 x SSC (high stringency). Hybrids were detected using streptavidin AP and NBT. Slides were examined using a microscope equipped with planapochromatic lenses. Pictures of the fungi using the different probes were obtained at 200× through a liquid crystal filter using a commercially available multispectral imaging system.

Results: All 3 probes identified fungal organisms in all cases. The LNA probe consistently produced the strongest signal under low and high stringency conditions. The LNA probe also had the most background staining but this was reduced following stringent washing. More organisms stained with the LNA probe. By MSI, the average signal intensity was highest for the LNA probe (0.78 (high stringency/0.72 low stringency) followed by the DNA probe (0.44 high stringency/0.37 low stringency) and lastly the PNA probe (0.37 for high and low stringency). The LNA probe produced a signal which was 1.7-1.9X the DNA probe and 1.8-2.1 times the PNA probe depending on the stringency. The DNA probe signal was found to be 1-1.2X the signal generated with the PNA probe.

Conclusions: DNA, LNA and PNA probes can identify pan-fungal rRNA sequences in tissues. Under the hybridization and washing conditions used in this study, the LNA probe resulted in a 2-fold level of intensity over PNA probe. Even though signal was weaker, in terms of the clarity of staining, the DNA probe compared well to the LNA probe and may be an alternative to LNA probes when one is using ISH for rRNA sequences in paraffin-tissues.

1745 Real-Time PCR Detection of MRSA and Other Staphylococci in Positive Blood Culture Bottles

S Mortuza, OV Martinez, TJ Cleary. University of Miami/Jackson Memorial Hospital, Miami, FL; University of Miami, Miami, FL.

Background: Coagulase-negative Staphylococci (CNS) and *Staphylococcus aureus* (SA) account for over 50% of all positive blood culture isolates at our institution. Staphylococcus bacteremia can cause significant mortality and morbidity in hospitalized patients; therefore, rapid identification of the Staphylococci and methicillin-susceptibility (MS) or resistance (MR) has been shown to improve patient care. We evaluated a multiplex PCR SybrGreen assay for the identification of SA, CNS, and MS/MR in 159 single patient blood cultures positive for Gram-positive cocci-in-clusters (GPC-Cl).

Design: One drop of blood culture fluid with GPC-Cl was added to a lysis tube containing 0.15 garnet beads (MO BIO, Carlsbad, CA) and 500ul of TRIS/EDTA buffer. The PCR master mix contained previously described oligonucleotide primer sets for the amplification of genes specific for the Staphylococcus genus (TStaG, 370bp, Tm 85°C), SA (SA442, 179bp, Tm 82°C), and MS (mecA, 98bp, Tm 79°C). The concentration of the various primer sets were weighted for the detection of SA and mecA. Amplification was performed in the SmartCycler instrument (Cepheid, Inc, Sunnyvale, CA). Three distinct peaks may be found by melt curve analysis of the amplified product. If the sample contained 3+ hemolysis after lysis, it was diluted 1:20 if the original PCR was negative.

Results: Of 18 patient samples positive for MRSA, PCR was positive in 17. The negative sample was identified as MRSA upon repeat testing of the original lysate. Fourteen patient samples were positive for MSSA. The two negative samples in this subset were identified as MS-CNS. These isolates may represent deletion mutations that are not detected by the SA442 PCR assay (JCM **41**:493, 2003).

Culture and PCR results from blood culture bottles

	MRSA	MSSA	CNS	>1 staphylococcal spp
Culture Positive	18	14	108	10
PCR Positive	17	12	104	10

CNS, alone, was found in 108 patient samples. Of these, 104 were detected by PCR. Two samples in this subset were positive for CNS when the original lysates were retested. Most species were MR. Ten patient samples were positive for two different Staphylococcal species. All of these samples were PCR positive. Nine patient samples grew organisms other than Staphylococci; none of these samples were PCR positive.

Conclusions: The real-time PCR assay was rapid, sensitive, and specific for the detection of MRSA in blood cultures with GPC-Cl. In addition, the assay also readily distinguished MSSA, CNS-MR, and CNS-MS.

1746 Expression of Natural Killer Receptors in T Lymphocytes and NK Cells Post Stem Cell Transplantation

H Olteanu, P Hari, BC Schur, SH Kroft. Medical College of Wisconsin, Milwaukee, WI.

Background: Limited information is available on the natural killer cell receptor (NKR) reconstitution in mononuclear cells after bone marrow transplantation (BMT). We studied the expression of NKRs on peripheral blood cytotoxic T lymphocytes and NK cells in patients who underwent an allogeneic BMT and compared these findings with results from a control cohort.

Design: Peripheral blood samples were collected from 20 normal adult volunteers and 15 allogeneic stem cell transplant patients. Mononuclear cells were prepared by whole blood lysis prior to flow cytometric analysis. Four-color flow cytometry was performed with antibodies against T and NK cell-associated antigens CD3, CD56, CD57 and the NKRs CD158a, CD158b, CD158e (also known as killer immunoglobulin-like receptors, KIR5) and CD94. Expression of NKRs was evaluated separately in CD56(+), CD57(+)

and CD56/CD57 (double +) subsets of T and NK cells, and compared in the two cohorts by the Mann-Whitney test.

Results: The mean absolute white blood cell count in the control group was 6,940 X 10^6/L, with mean T lymphocyte and NK cell percentages of 23% and 2.2%, respectively. The corresponding values in the BMT group were 5,980 X 10^6/L, 14% and 3.4%. CD158a and CD94 expression was variable, whereas CD158b and CD158e were generally detected on distinct subpopulations. The percentage of control cells expressing CD158a was significantly higher than in the BMT group in all subsets studied: CD56(+) T cells (41±3.9% vs. 28±3.2%, mean±SEM; p=0.02); CD57(+) T cells (44±3.0% vs. 29±3.5%, p=0.02); CD56/CD57 (double +) T cells (56±3.4% vs. 40±4.3%, p=0.02); CD56(+) NK cells (46±3.1% vs. 30±3.3%, p=0.001); CD56/CD57 (double +) NK cells (63±3.3% vs. 49±5.1%, p=0.05). CD158b and CD158e percentage and expression levels were similar in the control and BMT groups, with the exception of CD158b in CD56/CD57 (double +) NK cells (39±3.8% vs. 53±4.2%, p=0.03). Furthermore, the CD94 mean fluorescence intensity was significantly different in the CD57(+) T lymphocytes (129±24 vs. 45±5.9, p=0.0002) when comparing the controls with the BMT cohort.

Conclusions: Our study shows that T lymphocytes and NK cells in transplanted patients show differences in their NKR profile when compared to that of normal individuals, especially in CD158a expression. These preliminary results suggest that the immune reconstitution following BMT modulates NKR and CD94 expression differently in T and NK cells.

1747 Comparison of Multiplex Versus Non-Multiplex Primer Sets for the Detection of T-Cell Receptor-γ Gene Rearrangement

KP Patel, Q Pan, RW Maitta, J Du, H Ratech. Montefiore Medical Center, Bronx, NY.

Background: Multiplex PCR assays are often associated with decreased sensitivity due to a competition between the primers. This can be compensated by including a non-multiplex (simplex, single pairs) primer set in the test panel. We evaluated clinical utility of combining a non-multiplex PCR assay with a recently described multiplex assay (BIOMED-2 protocol) for T-cell receptor (TCR)-γ gene rearrangement (GR).

Design: A total of 144 consecutive samples received for TCR GR were subjected to PCR analysis using two sets of primers: (1) Multiplex BIOMED-2 primers for TCR-γ and TCR-β (van Dongen et al, 2003) and (2) Simplex primer sets for TCR-γ in a home-brew assay (Jaffe et al, 1995). PCR analysis for immunoglobulin heavy chain (IgH) GR was also performed on 62/144 cases. The results of TCR-γ GR by simplex and multiplex protocols were compared against those of TCR-β GR. Clinical and histological correlations were included in the interpretation of GR studies.

Results: The samples included skin biospies (101/144), bone marrow (19/144), blood (9/144) and other tissue (15/144). The results of TCR-β GR were considered as the gold standard for the evidence of TCR clonality. TCR-β showed clonal GR in 51/144 cases. The multiplex and simplex primers detected clonality in 33/51 and 37/51 TCR-β positive cases respectively, with 64.7% (multiplex) and 72.5% (simplex) sensitivity. Taken together, simplex and multiplex primers identified 41/51 TCR-β positive cases (sensitivity=80%). Overall, multiplex and simplex primers were in agreement in 121/144 (84%) cases. Out of 23/144 discrepant cases, clonality was detected in 8 cases with multiplex and in 15 cases with simplex primers. Out of 15 cases positive with simplex assay, 8/15 cases showed clonal TCR-β GR and 1/15 cases showed clonal IgH GR. The multiplex and simplex assay identified TCR-γ clonality in 16 and 19 cases respectively in TCR-β negative (93/144) cases. Analysis of discordant cases showed a wide range of presentations emphasizing the need to interpret the GR studies in the context of clinical and histological presentation.

Conclusions: Combining the multiplex BIOMED-2 primers with a non-multiplex primer set for TCR-γ increased the sensitivity of the T cell clonality assay. In addition, an independent confirmation of a positive or a negative multiplex assay by a set of non-multiplex primers adds to the clinical utility of TCR GR assay. Our study also highlights the real-life experience with cases showing ambiguous clinicohistologic findings.

1748 Array-Based Comparative Genomic Hybridization for the Detection of Genetic Aberrations in Cases of Congenital Anomalies and Developmental Delays

ML Petras, GJ Tsongalis. Dartmouth-Hitchcock Medical Center, Lebanon, NH.

Background: Traditionally, cytogenetic studies have been the main method for etiologic investigation of congenital anomalies, developmental delay, and mental retardation. High-resolution (5 megabases or greater) cytogenetic studies and fluorescence in situ hybridization (FISH) techniques have been the mainstay of these investigations; however, despite advances in techniques, the majority of cases go unresolved as to finding a responsible genetic abnormality. Array-based comparative genomic hybridization has become the new standard for analyzing the genome for microscopic and submicroscopic structural chromosomal imbalances and is able to detect DNA dosage alterations as small as a few thousand base pairs. Increased detection of genetic abnormalities leads to improved clinical diagnosis and subsequent patient management.

Design: A series of 642 cases of patients with developmental delay, dysmorphic features, seizure and metabolic disorders, autism and/or other developmental anomalies were sent for microarray analysis to Signature Genomics Laboratories, LLC, Spokane, WA. Peripheral blood samples were used in all cases. Samples underwent testing via either bacterial artificial chromosome (BAC) clones or oligonucleotide probes. All abnormalities were confirmed by FISH.

Results: Of these 642 patient samples, 106 cases demonstrated an abnormal result (a "hit rate" of 16.5%). The abnormal cases included both those with and without a known cytogenetic abnormality, thus improving detection rate of genetic anomalies. Turn-around-time for results averaged 6 days.

Conclusions: The use of array-based comparative genomic hybridization allows for an increase in the detection of cytogenetic anomalies in patients with developmental delay, dysmorphic features, seizure and metabolic disorders, autism and/or other developmental anomalies. This technique identifies a greater number of smaller chromosomal structural anomalies.

1749 An Objective Appraisal of Computerized Speech Recognition (CSR) in Final Routine Surgical Pathology Reporting

Z Qu, U Sivagnanalingam, B Forcione, U Sivagnanalingam, JS Van Vranken. University of Rochester, Rochester, NY.

Background: Recently, there is renewed enthusiasm of computerized speech recognition (CSR) in routine pathology work-flow. Since CSR has created repeated cycles of enthusiasm, frustration, and disappointment in the past ten years, there are diverse opinions on the usefulness or lack of it in routine pathology service. An objective appraisal/evaluation of CSR is eagerly awaited. We recently reported an outcome assessment of its application in surgical pathology with focus on gross examination. As the extension of the effort, this report focuses on the validity of CSR in routine pathology diagnosis reporting/sign-out.

Design: CSR and transcriptionist-assisted documentation (TAD) are compared for 7 parameters (see table). Parallel routine sign-out and simulation experiment are designed for the outcome assessment/appraisal. In the former, 186 surgical cases and 531 surgical cases are included in CSR and TAD, respectively. In CSR simulation arm, prior reports of 76 cases are repeated by three different users. Four participating users include a pathologist with >10-year CSR experience, and three students with >12 hours of general and pathology CSR training. Dragon Naturally Speaking version-9, (Nuance Inc.) is used for CSR. Time is recored by stop-watch. Error rate is recorded manually. Multivariant statistical analysis is used. No built-in macros are used in this study.

Results: For pathologist, CRS seems to require slightly more dictation time, but takes less total time to complete the diagnosis reporting than TAD:

Results of Comparing CSR and TAD

Parameters	CSR	TAD
Case number	474	571
System involved	1	2
Steps Required	4	7 + ≥ 1
Dictation Speed (sec /slide)	15.9 +/- 1.9	14.8 +/- 2.2
Efficiency (words/minute) *	61.80+/-13.8	68.88+/-12.06
Accuracy rate	97.7 +/- 2.2%	98.7 +/- 1.2%
Overall Time (sec/slide) *	70.4+/-12.3	83.0+/-19.2
RTAT	<2 minutes	≥ 2.5 hours

RTAT: Relative turn around time -- from the final diagnosis rendered by voice input till release of the final report. Overall Time: total time required to complete reporting by pathologist. Transcriptionist's efforts are not included in the result table. * p value <0.05

Conclusions: CSR requires less time overall on pathologist's part in reporting final diagnosis, mainly by eliminating additional steps associated with TAD. The objective assessment provides tangible evidence of the value of CSR in routine pathology diagnosis reporting. More work is needed to complete the appraisal.

1750 Diagnostic and Prognostic Significance of High Hyperferritinemia in Hemophagocytic Syndrome

RC Reed, K Hutchinson, PM Rainey, MH Wener. University of Washington, Seattle, WA.

Background: Hemophagocytic syndrome (HPS) and Still's disease (systemic onset juvenile chronic arthritis) present a diagnostic challenge, since many symptoms are nonspecific. An important diagnostic tool is the serum ferritin concentration, which can reach levels in excess of 100,000 ng/mL. However, the sensitivity and prognostic significance of high hyperferritinemia in the diagnosis and evaluation of HPS has not been examined. Additionally, the ferritin immunoassay is subject to a high dose hook effect at these concentrations, potentially confounding interpretation of this value.

Design: We examined the characteristics, including eventual diagnosis and survival time, of patients with high hyperferritinemia showing a hook effect (>99,000 ng/mL), drawing from the results of 37,185 ferritin tests performed over a three-year period. Hook effect was further investigated experimentally, to characterize the performance of the ferritin immunoassay.

Results: Nine patients, with a total of 15 (0.04%) clinical samples, had ferritin levels greater than 99,000 ng/mL, sufficient to yield a hook effect. Of eight patients for whom clinical information was available, six had documented HPS; of these, 4/6 were likely related to EBV or CMV infection, and 2/6 were secondary to hematologic malignancy (one T-cell lymphoma and one NK cell leukemia). Another patient presented with acute hepatitis, possibly ischemic, and one patient with bacterial endocarditis and subarachnoid hemorrhage exacerbating chronic diabetic renal disease. Five of the eight died less than a month after presentation with hyperferritinemia, while two with viral-related HPS are alive at least one year after diagnosis, and the patient with acute hepatitis was discharged in good condition. The hook effect threshold was similar in patient and experimental samples, with assay results decreasing predictably as the ferritin concentration increased. To avoid reporting falsely low results due to the hook effect, samples with results >300 ng/mL can be automatically diluted and repeated. At this cut-off, ferritin concentrations up to >500,000 ng/mL are accurately detected.

Conclusions: HPS and Still's disease are diagnostic challenges, and hyperferritinemia is an important criterion. High hyperferritinemia predicts HPS in our series, though acute hepatotoxicity and other inflammatory conditions may also yield very high ferritin concentrations. Ferritin levels above ~100,000 ng/mL were associated with a high mortality rate. We describe a new, automated method to detect and prevent hook effect.

1751 A Tumor-Targeted DNA Extraction Method for Array CGH Analysis of *HER2* Gene Copy Number Status in Newly Diagnosed Breast Cancer

RS Robetorye, SR Gunn, I Yeh. University of Texas Health Science Center at San Antonio, San Antonio, TX; Combimatrix Molecular Diagnostics, Ir, CA.

Background: Array-based comparative genomic hybridization (array CGH) is currently actively being evaluated as a clinical tool for the rapid and accurate evaluation of *HER2* gene copy number status in newly diagnosed breast cancer. However, currently validated array CGH assays require tumor-targeted high molecular weight (HMW) DNA extraction from fresh or frozen breast tumor tissue. While tumor-targeted DNA extraction insures that the tumor genome is evaluated by array CGH, visualization of the tumor by H&E staining of tissue prior to DNA extraction necessitates transport media that preserves both tissue architecture as well as DNA quality.

Design: Twenty frozen breast cancer samples previously evaluated for HER2 status by array CGH [HER2 positive (n=10)] and [HER2 negative (n=10)] were thawed and stored for at least 48 hours in RNA*later* (Applied Biosystems, Foster City, CA). Samples were re-frozen and sectioned for H&E staining followed by tumor-targeted DNA extraction for array CGH analysis. Results from the RNA*later* processed samples were compared to results obtained from non-processed samples.

Results: In all cases, high-quality HMW DNA was obtained for array CGH analysis and *HER2* copy number was concordant with previously determined HER2 copy number results.

Conclusions: Fresh and/or frozen tissue from newly diagnosed breast cancer can be obtained at the time of surgery and preserved for future tumor-targeted DNA extraction and array CGH evaluation of *HER2* gene copy number status. This analysis algorithm makes it possible to store and/or ship samples for 48 hours or more before subsequent histological examination and array CGH analysis is performed.

1752 Digital v. Routine Microscopic Assessment of Prostate Needle Biopsies (NB): An Initial Reproducibility Study

PA Rodriguez-Urrego, A Gopalan, SK Tickoo, AM Cronin, VE Reuter, SW Fine. Memorial Sloan-Kettering Cancer Center, New York, NY.

Background: Recent advances in whole slide imaging technology have raised the prospect of using digital imaging for routine diagnostic applications. Few studies however, have evaluated concordance of routinely reported parameters between routine (glass slides) and digital media.

Design: 50 cancer-bearing prostate NB with varying Gleason scores (GS) and cancer volumes were selected. For each, a single level was marked on the glass slide and scanned with an automated whole slide imaging device. Four urologic pathologists reviewed digital and glass slides (≥ 1 week apart), without access to clinical reports/consultation. For each NB, 1° and 2° Gleason grades (GG), GS, % and mm of tumor, and perineural invasion (PNI) were recorded and agreement between subjects and methods of assessment was calculated using the kappa statistic of agreement.

Results: Interobserver Agreement (pathologists): For both routine and digital assessment, at least 3 of 4 pathologists were in accord for 1° GG in > 85% of cases [κ of 0.70, 0.64]. Assessment of 2° GG [κ of 0.40, 0.35] and GS [κ of 0.55, 0.53] was more variable, yet achieved good agreement across media; GS agreement was slightly enhanced when clinically meaningful categories (≤6 v. 7 v. ≥ 8) were used [κ of 0.63, 0.56]. With both methods, at least 3 pathologists had exact concordance for PNI in ≥ 90% of cases [κ of 0.50, 0.65]. Superior agreement was achieved for mm of cancer (grouped by 1 mm intervals) [κ of 0.47, 0.65] than for % cancer (grouped by 10% intervals) in each method of assessment [κ of 0.36, 0.42]. Intraobserver Agreement (modes of assessment): All pathologists had excellent agreement [κ > 0.7] for 1° GG. Concordance for 2° GG was lower for all pathologists, but achieved κ > 0.55 for 3 of 4 subjects. For GS, all pathologists had favorable agreement [κ of 0.51, 0.76, 0.76, 0.77] and concordance for PNI was similar [κ of 0.42, 0.53, 0.81, 0.84]. Every pathologist achieved better agreement for mm of cancer than for % cancer.

Conclusions: Good to excellent agreement was achieved for all Gleason parameters and perineural invasion across both methods of assessment. Superior levels were attained for primary Gleason grade and clinically important Gleason score groups, while size of cancer was a more reproducible parameter than % cancer across both media and all study subjects. These findings indicate that digital assessment of prostate NB is feasible and may further improve with increased experience.

1753 Novel Algorithm for Analyzing Whole Genome Amplified DNA for SNP Array Analysis

MA Sajid, X Zhou, W-T Huang, C-C Chang. The Methodist Hospital, Houston, TX; The Methodist Hospital Research Institute, Houston, TX.

Background: Applying whole genome amplification to some fractions is required to generate enough DNA material for single nucleotide polymorphism (SNP) array analysis using the sorting approach. Using whole genome amplification, noise is amplified decreasing the signal noise ratio (SNR) of log2-ratio values.

Design: To reduce the influence of noise, we propose a conditional random pattern (CRP) model for copy number inference using amplified DNA samples. In CRP model, the current hidden state (real copy number) is determined by its two immediate neighboring hidden states, and a continuous segment of observations (log2-ratios). We evaluated the feasibility of using the amplified DNA for SNP array analysis by Pearson correlation of log2-ratio values between whole-genome amplified DNA and un-amplified DNA. The calculated Pearson correlation coefficient between un-amplified and amplified DNA samples is about 0.81. We then applied dChip, CNAG and CRP model to 6 SNP arrays of myelodysplastic syndrome (MDS) samples after whole-genome amplification. dChip and CNAG are academic softwares for SNP array analysis. Copy number inference results using dChip, CNAG and CRP model in a case with trisomy (Chromosome 8) and a case with monosomy (Chromosome 7), as determined by conventional cytogenetic studies and by SNP array analysis using non-whole-genome amplified DNA of the same patient, were compared.

Results: The results showed that dChip and CNAG, but not CRP, miss many gain regions in chromosome 8 and deletion regions in chromosome 7. Additionally, dChip and CNAG detected about 100 copy number aberration (CNA) regions in other chromosomes in both cases, with 19 of them consisting of only one SNP locus. Most of these changes are not observed when the data are analyzed by CRP or when the SNP array using non-amplified DNA of the same patients were analyzed by dChip, CNAG or CRP.

Conclusions: These results indicated that the CRP model we developed generates more accurate results using amplified DNA samples than dChip or CNAG.

1754 "Xpress™"-ed Tissue Materials for Molecular Surgical Pathology

A Serizawa, T Itoh, N Kato, H Itoh, RY Osamura. Tokai University School of Medicine, Isehara, Japan.

Background: Recently, it has been recommended to rapid-process the surgical materials in order to expedite the pathology reporting. It has to be pointed out that these rapidly processed tissues are not infrequently subjected to the molecular studies for more accurate diagnosis, prognosis and for molecular targeted therapy. This study is aimed at to elucidate whether rapidly processed and paraffin embedded tissues are suitable for molecular analysis, FISH amplification, mutational analysis and RT-PCR.

Design: Biopsied or surgically resected specimens were subjected immediately to Xpress™-x50(Sakura Finetek), which uses microwave fixation. Whole processing into paraffin require approximately 40minutes. After regular H&E staining, the entire through-put is less than two hours. The Xpress™-x50-processed paraffin embedded sections were subjected to the following molecular analysis, EGFR FISH, EGFR mutation, p53 mutation and real time RT-PCR. Results were compared with those by FFPE materials.

Results: From the "Xpress™-x50"-ed tissue sections, pulmonary bronchiloalveolar carcinoma(BAC) showed EGFR Point mutation (CGCàCCC) in Exon21 at 26th : Arg832Pro, or Point mutation (GTCàATC) in Exon19 at 40th : Val742Ile. EGFR FISH showed comparable ratio of EGFR/CEP17 to that of FFPE. P53 point mutation (CGCàCAC) in Exon7 at 71th : Arg248His was detected in colorectal cancer. These molecular changes were exactly comparable to those by FFPE section. Recovery of mRNA is appreciable, even though less than that of fresh frozen or FFPE materials.

Conclusions: Our studies showed that rapidly processed tissues could be subjected to molecular studies such as mutation analysis, FISH and RT-PCR. For prognostication and therapeutic application, molecular analyses can be also expedited using this technique in order to provide appropriate personalized therapy without delay.

1755 HPV Status Using the Third Wave Technologies Invader® HPV ASR Compared to the Digene Hybrid Capture 2 Assay

S Sethi, CL Bartels, SL Gallagher, BJ Dokus, A Hawk, SA Feher, GJ Tsongalis, V Padmanabhan. Dartmouth Hitchcock Medical Center, Lebanon, NH.

Background: Testing for high-risk (HR) HPV in conjunction with Pap-tests is now the standard of care in the U.S. With increased demand for HPV testing there is need for more automated testing solutions. In this prospective study we compared the performance of the Invader® HPV ASR and the Tecan EVO 150 workstation (Hologic, Marlborough, MA previously Third Wave Technologies, Madison, WI, USA), a more automated process to the routinely used Digene Hybrid Capture 2 (HC2) assay.

Design: Three probe pools (A5/A6 [51, 56, 66], A7 [18, 39, 45, 59, 68] and A9 pool [16, 31, 33, 35, 52, 58]) in the Invader® assay (detects 14 HR HPV types) were used using using a Tecan EVO 150 workstation and Invader® HPV ASR reagents. Limit of detection was determined by diluting plasmids for each genotype in SurePath™ media from normal cytology samples. Diagnostic accuracy and precision were determined using 245 previously tested raw specimens that were submitted in SurePath™ liquid-based cytology medium for routine HR HPV DNA testing using the Hybrid Capture 2 (HC2) assay (Digene, Gaithersburg, MD). Additionally, enriched Surepath specimens were also evlauted. Sample extraction was performed using the Agencourt Genfind magnetic bead separation method.

Results: For the enriched samples the sensitivity was 97.1%, specificity 100%, and accuracy 98.4%. Of the 245 diluted samples tested, 208 (85%) were concordant between the two methods. Five samples did not have a sufficient quantity of specimen, 1 was inhibited and 1 had a dilution error. Thirty-seven samples (15%) were discordant. These cases were HC2 positive and Invader® negative resulting in a sensitivity of 95.6%, specificity of 87.6% and accuracy of 90.7%. All Digene HC2 control samples, negative calibrator in triplicate, positive HR calibrator in triplicate, positive control, and negative control gave expected results. All Invader® controls (3 different subtype pools and a histone DNA control) gave expected results.

Conclusions: The combination of the Tecan EVO 150 and the Invader® chemistry is a robust method for HPV detection in liquid based SurePath cytology specimens and results in less hands-on time than the Digene HC2 assay. Enriched liquid cytology specimens gave superior performance characteristics.

1756 Quality Control of Human Tissues Used in Research Studies

Y Shim, J Deeds, R Meyer, M-H Ryu, L Ostrom, P Fordjour, D Ruddy, S Kamatkar, J Monahan, R Mosher. Novartis Institute for Biomedical Research, Cambridge, MA.

Background: High quality tissue collections are required for human tissue based research. Tissue quality can be markedly affected by handling prior to fixation or freezing. When tissues are acquired from a variety of sources a QC quality control method must be standardized to ensure consistent experimental data. We present our QC data from frozen and FFPE tissues collected across a variety of sources.

Design: We collected 1985 human tissues in total, 883 in FFPE (344 in normal and 539 in tumor) and 1102 in frozen (529 in normal and 573 in tumor), in 24 different tissue types from 9 different tissue sources between Mar. 2005 and Jun. 2008. Each sample was HandE stained and samples were excluded based on poor composition or autolysis. For protein QC, IHC staining against pSTAT3 antibody was performed on FFPE samples and for RNA QC, RNA was extracted from frozen samples. We only analyzed the data for a subset of tissue sources and tissue types (4 different tissue sources and 5 different tissue types with greater than 50 samples). Normal frozen samples were excluded from this analysis. Positive pSTAT3 staining indicates protein QC pass and good RNA quality indicates RNA QC pass.

Results: pSTAT3 and RNA results by tissue source and tissue type are shown in Table1 and 2. Among different tissue sources, the pSTAT3 QC pass rate varied from 87% – 92% and the RNA QC pass rate varied from 80% – 88%. Among different tissue types, the pSTAT3 QC pass rate also varied from 86 % – 91% and the RNA QC pass rate varied from 79 % – 94%. There is a significant percentage of N/A due to no data available, tissue not processed, tissue processed but yield too low or no RIN detected for RNA QC.

Table 1. pSTAT3 results by Tissue Source & Tissue Type

pSTAT3	Source 1		Source 2		Source 3		BREAST		COLORECTAL		KIDNEY		LUNG	
positive	507	87%	110	87%	66	92%	223	86%	179	91%	113	87%	71	91%
negative	26	4%	17	13%	6	8%	12	5%	4	2%	17	13%	6	8%
N/A	50	9%	0	0%	0	0%	23	9%	13	7%	0	0%	1	1%
Total	583	100%	127	100%	72	100%	258	100%	196	100%	130	100%	78	100%

Table 2. RNA results by Tissue Source & Tissue Type

RNA Quality	Source 1		Source 2		Source 4		BREAST		COLORECTAL		KIDNEY		LUNG		STOMACH	
good	211	85%	168	88%	98	80%	126	79%	106	91%	70	90%	66	90%	79	94%
bad	5	2%	5	3%	1	1%	2	1%	4	3%	1	1%	1	1%	2	2%
N/A	32	13%	18	9%	23	19%	32	20%	7	6%	7	9%	6	8%	3	4%
Total	248	100%	191	100%	122	100%	160	100%	117	100%	78	100%	73	100%	84	100%

Conclusions: 1. Variation in quality of protein and RNA among different tissue sources and tissue types was observed but overall the sample quality was good. 2. In general, the quality of breast samples was lower for both protein and RNA. 3. It is recommended to have on-site QC done.

1757 Overexpression of CD49f in Precursor B-Cell Acute Lymphoblastic Leukemia: Efficiency of Minimal Residual Disease (MRD) Detection by Flow Cytometric Immunophenotyping Compared with Commonly Used Markers

H Shinoda-Matsuoka, JA DiGiuseppe. Hartford Hospital, Hartford, CT.

Background: The persistence of minimal residual disease (MRD) following therapy is an established prognostic factor in precursor B-cell acute lymphoblastic leukemia (pB-ALL). Detection of MRD in pB-ALL by flow cytometric immunophenotyping (FCM) requires demonstration of abnormal antigen expression in leukemic B-cell precursors relative to that of normal B-cell precursors (hematogones). We have recently shown that CD49f (integrin alpha-6) is commonly overexpressed in pB-ALL relative to normal B-cell precursors, and represents a potentially useful marker for the immunophenotypic detection of MRD (DiGiuseppe JA, et. al. *Cytometry Part B*; in press). However, the efficiency of MRD detection using CD49f has not been compared with that of more commonly used markers, such as CD10, CD13, CD33, CD38, and CD58.

Design: We studied a series of 25 patients (median age: 5 years) with pB-ALL in whom residual disease was detectable (i.e., >0.01%) at one or more times following induction chemotherapy. Expression of CD49f, as well as CD10, CD13, CD33, CD38, and CD58, was evaluated by 4-color FCM in bone marrow aspirate samples, and compared with expression of each of these antigens in normal B-cell precursors. In order to be considered abnormal, expression of a given antigen was required to be recognizably distinct from that of normal B-cell precursors by visual inspection of dot plots, with at most minimal overlap in fluorescence intensity.

Results: CD49f was overexpressed in 22 of 25 (88%) cases. The proportion of cases with abnormal CD49f expression was significantly higher than the proportions observed using CD10, CD13, CD38, and CD58 (Table 1); comparison with aberrant CD33 expression approached, but did not reach, statistical significance.

Table 1

Antigen	CD10	CD13	CD33	CD38	CD58	CD49f
# of abnormal/ total# of cases	6/25	15/25	16/25	9/25	13/25	22/25
% of abnormal cases	24	60	64	36	52	88
p value vs. CD49f	<0.01	0.02	0.07	<0.01	0.01	N.A.

Moreover, in informative cases, the difference in intensity between CD49f expression in leukemic blasts relative to normal B-cell precursors was typically dramatic, facilitating detection of MRD by visual inspection of dot plots.

Conclusions: The efficiency of CD49f overexpression as a marker of MRD in pB-ALL compares favorably with that of markers commonly used in current practice, suggesting that CD49f may be a useful addition to existing antibody panels.

1758 A Double Immunostaining Technique with a Cocktail CK5, CK14, p63, CK7 and CK18 Distinguishes between Hyperplasia of the Usual Type, Atypical Hyperplasia, Microinvasive and Basal Phenotype Breast Cancers

DE Tacha, K Bloom, A Kyshtoobayava, S Gofstein. Biocare Medical, Concord, CA; Clarient, Aliso Viejo, CA.

Background: The aim of the study is to examine immunohistochemical staining characteristics in benign proliferative breast disease, noninvasive breast malignancies and invasive breast cancers. In breast cancer, immunohistochemical classification of hyperplasia of the usual type verses atypical hyperplasia that can be difficult to diagnose. A rapid 4-step double-immunostain technique was developed to characterize a spectrum of intraductal epithelial proliferations, namely benign usual ductal hyperplasia, atypical ductal hyperplasia, microinvasion and ductal carcinoma in situ. An antibody cocktail of CK5, CK14, p63, CK7 and CK18 was designed to see if we could distinguish invasive from non-invasive breast lesions with the presence or absence of myoepithelium (CK5/14 and/or p63) (DAB) and glandular staining of breast cancer with CK7/CK18 (Fast Red).

Design: Monoclonal antibodies CK5, CK14, p63 and rabbit monoclonal antibodies CK7 and CK18 were optimally tittered and validated for specificity and staining intensity. All 5 antibodies were cocktailed into a single antibody componet and applied on TMA breast tissues. A double stain detection reagent composed of goat-anti-mouse-HRP and goat anti-rabbit-AP was applied, folllowed by DAB and Fast Red chromogens.

Results: Staining patterns distinguished invasive from non-invasive breast lesions with the presence or absence of myoepithelium (CK5/14 and/or p63) (DAB) and glandular staining of breast cancer with CK7/CK18 (Fast Red). Usual ductal hyperplasia appears to be a CK5/14-positive committed stem (progenitor) cell lesion; thus both CK/5/14 and luminal CK7/18 was observed. This is in sharp contrast to atypical ductal hyperplasia/ ductal carcinoma in situ, which display the differentiated glandular immunophenotype (CK7/CK18-positive, but was CK5/14 negative). Microinvasive breast cancer was more easily identified as invasive tumor cells were CK7/CK18 (red) positive. Basal phenotypes were mostly high-grade and consistently showed expression of CK5/14 (DAB).

Conclusions: This quintuple antibody cocktail has great utility and can be used for the interpretation of benign usual ductal hyperplasia, atypical ductal hyperplasia, microinvasion and ductal carcinoma in situ, all of which are thought to represent a gradual sequence in developmental breast cancer. This procedure can be used manually or on an automated staining platform.

1759 Assessing HER-2/*Neu* Protein Expression and Gene Alteration in Gastric Cancer: Comparing Arrayed Comparative Genomic Hybridization (aCGH) Technique with Immunohistochemistry (IHC) and Fluorescent In-Situ Hybridization (FISH)

CD Truong, W Feng, W Li, T Khoury, J Yao, K Xie, D Tan. The University of Texas MD Anderson Cancer Center, Houston, TX.

Background: Inconsistent results for HER-2/*neu* expression (at the protein or gene level) in gastric cancer using IHC and FISH and Herceptin's promising role in the treatment of gastric cancer have been reported in several studies. These inconsistencies may partially be due to variation in evaluation techniques and/or heterogeneity of the populations studied. The objective of this study was to assess HER-2/*neu* expression using aCGH in a well-defined large cohort of gastric cancer patients, and to compare this novel technique with the traditional approaches of IHC and FISH under uniform test conditions.

Design: Tissue samples from 200 patients with primary gastric cancer were evaluated by IHC analysis (using an FDA-approved Hercept monoclonal antibody kit) and FISH with standard score criteria used for both methods. Among this cohort, 43 cases had adequate tissue for assessing DNA copy number changes by oligonucleotide aCGH (244K, Agilent). For each aCGH probe, each sample was classified as having normal, gained, or lost DNA copy number based on log 2 ratio thresholds of ±0.15.

Results: Twenty patients (10%) overexpressed (2+, 3+) HER-2/*neu* protein, while 90% showed negative (0, 1+) expression. Eighteen patients (9%) displayed HER-2/*neu* gene amplification by FISH. Although HER-2/*neu* protein overexpression was found to correlate well with HER-2/*neu* gene amplification (r=0.83, p<0.01), we found discordances in 3 cases. One case with negative (1+ by IHC) expression showed HER-2/*neu* amplification by FISH. Two cases with overexpression (2+ by IHC) did not show HER-2/*neu* amplification by FISH. On the other hand, aCGH detected HER-2/*neu* amplification in 16% of cases, of which 3 cases were negative by IHC and FISH. In addition to identifying HER-2/*neu* gene amplification, aCGH also displayed abnormalities of other associated critical genes, such as *DACT3, DKKL1, EGFR, EMP3, HIF3A, HRC, IGFL2, IGFL3, KPTN, LIG1*, and *PNKP*, many of which have been implied in the carcinogenesis of solid tumor including gastric cancer.

Conclusions: Although IHC and FISH offer direct *in-situ* assessment of molecular changes within the cells of interests, genome wide aCGH is more superior. In addition to having higher sensitivity in detecting HER-2/*neu* gene amplification, aCGH can also reveal a panel of associated gene changes, which may be more beneficial in personalizing treatment using multi-target therapy.

1760 Diagnosis of Cutaneous Herpesvirus Infections from Paraffin-Embedded Tissue Using PCR

G Turner, K Pesavento, C Sutherland, KL Kaul, TA Victor. Evanston Northwestern Healthcare, Evanston, IL.

Background: Both primary and reactivated Herpes-family virus infection can result in cutaneous lesions. Knowledge of which Herpesvirus is causing clinical symptoms can be important in immediate and long-term treatment. It is impossible to differentiate between lesions caused by Herpes Simplex Virus 1 (HSV-1), Herpes Simplex Virus 2 (HSV-2) and Varicella Zoster Virus (VZV) via routine H&E light microscopy. Although IHC stains for HSV-1/HSV-2 and VZV are commercially available, they have shown limited usefulness in our IHC lab. Real-time PCR assays for the detection and differentiation of these viruses have become widely available. This study examines the ability of PCR to detect and discriminate various Herpesvirus family members in paraffin-embedded skin lesions.

Design: Paraffin-embedded tissue blocks for 23 skin biopsy specimens with "Herpes Virus" in the diagnosis text were retrieved. Of these, 13 were clinically suspect for Herpesvirus infection, 21 were diagnosed histopathologically as Herpesvirus infection (VZV or HSV) or consistent with Herpesvirus infection, and 2 were diagnosed as possible Herpesvirus infection. Sections from each were stained with antibody against HSV-1/HSV-2 (Ventana Medical Systems, #760-2648) and against VZV (Novocastra, clone C90.2.8). DNA was extracted from paraffin-embedded tissue and analyzed by real-time PCR for HSV-1/HSV-2 and VZV using commercial and in-house-developed ASR reagents, respectively.

Results: Of the 23 specimens, IHC and PCR were in agreement for 12 cases. 7 were HSV positive/VZV negative by both IHC and PCR. 3 were VSV positive/HSV negative by both approaches and 2 cases were entirely negative. Among the cases with discrepant results, 1 was positive for HSV by PCR but not IHC. 6 were positive for VZV by PCR but not by IHC. 4 cases demonstrated mixed positivity for HSV and VZV by IHC and/or PCR.
Conclusions: Real-time PCR performs similarly to IHC in the detection of HSV in formalin-fixed paraffin-embedded skin biopsy specimens. Real-time PCR appears to be more sensitive than IHC in the detection of VZV. Several specimens demonstrated the unexpected finding of mixed positivity by both IHC and PCR. Real-time PCR can serve as an important tool in the identification of Herpesvirus family members from paraffin-embedded tissue.

1761 Raman Imaging Technique for Prostate Cancer Prognostication: A Feasibility Study

AH Uihlein, AJ Drauch, JS Maier, JK Cohen, PR Olson, JS Silverman. Allegheny General Hospital, Pittsburgh, PA; ChemImage Corp., Pittsburgh, PA.
Background: Raman Molecular Imaging (RMI), a technique used primarily in chemical analysis, is based on the scattering of laser light. RMI yields an image of a sample wherein each pixel of the image is the Raman spectrum (RS) of the sample at the corresponding location. The RS generates data reflecting the local chemical environment of the sample at each location. RMI has a spatial resolving power of 250 nm and can potentially provide qualitative and quantitative image information based on molecular composition and morphology. We have previously applied RMI as a reagentless tissue imaging method for the analysis of pathology specimens. In this study, we investigated the application of RMI on radical prostatectomies specimens with Gleason Score 7 prostate cancer (GS7 PCa), as a tool for prognostication, since the majority of GS7 PCa will be surgically "cured", but a significant number (~20%) will progress.
Design: Our study evaluated whether RMI can be used to differentiate GS7 PCa that subsequently progress (PROG) from those that have no evidence of disease (NED) after 5 years. Raman images were generated from unstained sections of 10 PROG patients and 10 NED patients. Measurements derived from RMI of tissue samples were analyzed using multivariate techniques established in analytical spectroscopy. We applied Mahalanobis Distance Analysis (MD), a chemometric method that measures distance between data sets in RS, for our study.
Results: Establishing PROG and NED as two different classes and performing Principal Component Analysis (PCA) of the 68 spectra derived from RMI, allows calculation of MD between the two classes. This evaluation shows a clear distinction between PROG and NED data. A two-sample z-test applied to the PCA scores has a p value of less than 0.01, confirming a significant difference between the two groups of GS7 PCa patients (progressive disease vs. no evidence of disease after 5 years). All cases of GS7 cancer were confirmed based on histopathologic findings.
Conclusions: RMI shows potential to distinguish between GS7 PCa that will eventually progress and those with no evidence of disease on follow-up, thus complementing current prognostic methodologies. RMI represents a novel analytical technique that may be able to assist in predicting tumor behavior and the need for adjuvant treatment.

1762 Quantitative Immunohistochemistry Methods Development for ER Detection in Breast Cancer

KA Vanpatten, M Loftus, J Pettay, L Wang, S Estrada, N Haubein, GS Lett, P Miller, R Tubbs, GA Pestano. Ventana Medical Systens (a Member of the Roche Group), Tucson, AZ; Lerner College of Medicine, Cleveland, OH; The BioAnalytics Group, Jamesburg, NJ.
Background: The assessment of cancer biomarker status in tissues represents a critical component in the development of therapeutics as well as in diagnostics. However, tissue-based diagnostics are often subjectively assessed. In addition, manual methods for slide processing promote inconsistency, are labor demanding and time-consuming. Automated IHC and ISH in formalin-fixed paraffin-embedded (FFPE) tissues allows standardized, rapid evaluation of gene and protein biomarkers in a high-throughput format. Further, advances in detection, including multiplexed Quantum dots (Qdots®), and spectral imaging, provide a growing set of tools that could complement biomarker studies.
Design: We have applied automated IHC methods with Qdot detection and image analysis to monitor markers in FFPE tissues that may be therapeutic targets, prognostic of disease, or surrogates of drug response. Software algorithms were developed in this study to aid in the deconvolution of hyperspectral data, and to identify cells and cellular compartments. In the study of breast cancer specimens, samples were analyzed for the simultaneous detection of QD 605 CK (cytokeratin), QD 655 ER (estrogen receptor), and the nuclear marker, DAPI. Dual stained CK/ER Qdot IHC results were assessed for concordance with pathology scores, single-stained chromogenic image analysis assays, as well as by qRT/PCR for detection of the estrogen receptor.
Results: The Spearman Rank Correlation test was used to compare chromogenic pathology scores with Qdot image analysis results. Specifically, Qdot detection of ER expression correlated with a statistically significant p value of 0.0003 (rank correlation = 0.927) to the pathology scores. We also noted that significantly enhanced dynamic range of antigen detection was achievable with Qdot detection in FFPE.
Conclusions: In this study we have demonstrated technical feasibility of using multiplexed Qdot IHC coupled with quantitative image analysis. The automated image analysis methods correctly identified ER potein levels, and were consistent with pathology review in breast cancer specimens. These results indicate that advanced analytical methods may be applied to breast cancer biomarker assessment in routinely collected FFPE tissues, but only when using highly standardized techniques.

1763 Integrating Image Analysis into the Pathology Workflow: Reduced Opportunities for Errors and Improved Efficiency

MR Verardo, RL Ryan, S DeVore, J Schmid. Dako North America, Carpinteria, CA.
Background: The modern pathology laboratory has the challenge of performing more work with fewer resources, while still producing quality results. Integrating efficient workflow solutions into the pathology laboratory is one example of a solution to this challenge. The steps used to produce a slide for viewing by a pathologist have been considered to be part of the pathology lab workflow. However, integrating imaging and image analysis into this workflow has traditionally been overlooked. Here we describe the design of an integrated image analysis workflow into the pathology laboratory.
Design: Slides were processed by AutostainerLink instruments using the DakoLink middleware manager software. A Dako Automated Cellular Imaging System (ACIS) III® was also connected to the DakoLink middleware system. Image analysis applications were used for analysis. Following this analysis by a pathologist of the digital slides, reports were generated. This workflow was compared to the traditional model of evaluating slides on a manual microscope and writing a pathologist report. The number of data entries and number of characters in both the automated workflow and manual imaging workflow was recorded.
Results: The number of times the information for a slide was re-entered or re-written was reduced. Also, the number of points where errors could be introduced into the pathology workflow was reduced following the integration of imaging and image analysis into the workflow. Also, by incorporating slide scanning into "off times" and incorporating image analysis into working hours, efficiency was increased overall for digital imaging.
Conclusions: By integrating workflow concepts into imaging and image analysis the opportunity for errors can be reduced while increasing efficiency by using instruments in traditionally "off times" and through parallel processing. Thus, a solution to new constraints in the pathology laboratory, that also increases overall performance (as measured by reduced opportunity for errors), is the integration of imaging and image analysis into automated pathology workflows.

1764 A Simple and Flexible Device To Pour the Holes in Paraffin Tissue Microarrays

UF Vogel. University Hospital, Eberhard Karls University, Tuebingen, Baden-Wuerttemberg, Germany.
Background: Paraffin tissue microarrays (PTMAs) are constructed by injecting paraffin tissue core biopsies (PTCBs) into preformed holes in a recipient block. These holes can be punched (Kononen), drilled (Vogel) or poured (Mengel). Devices to pour the holes normally consist of a modified steel mold with steel pins at the bottom (Figure 1A; TMA builder, LabVision). So, the size of the recipient block and the arrangement and the number of the holes are determined by the steel mold. To make the system more flexible and to reduce the manufacturing cost I designed a simple device which uses ordinary steel molds of different size, spacer plates with steel pins and a perforated plate. In contrast to the modified steel molds the steel pins are placed from above into the ordinary steel mold.
Design: Spacer plates (nickel silver) were equipped with different numbers of steel pins (length: 16 mm; diameter: 1.0 mm) in different arrangements (Figure 1C; S spacer plate; maximum amount of steel pins). A perforated plate (nickel silver) was constructed corresponding to the spacer plate with the maximum amount of steel pins (Figure 1C; P perforated plate). Different ordinary steel molds (tissue-tek) (Figure 1C; M mold), a plastic cassette (optional)(Figure 1C; C cassette), the perforated plate and different spacer plates were put together like a sandwich (Figure 1B) and filled with liquid paraffin. After solidification, the sandwich was disassembled to release the recipient block (Figure 1C; R recipient block). Paraffin tissue core biopsies were manually injected into the holes of the recipient block. The PTMAs were cut and the sections were stained according to routine procedures.

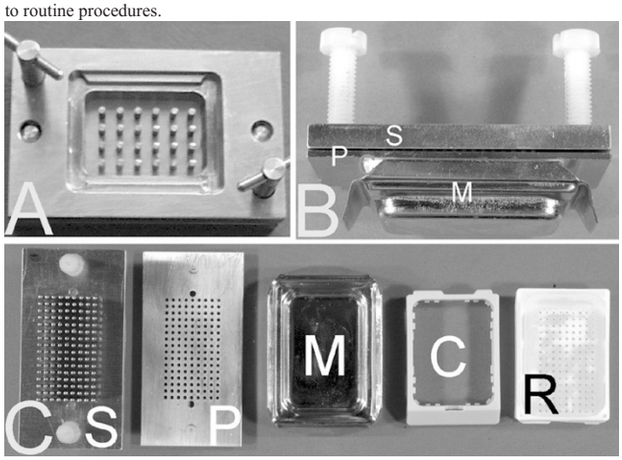

Results: PTMAs with different size and with different numbers and different arrangements of the PTCBs were successfully constructed.
Conclusions: With the novel device consisting of spacer plates and a perforated plate it is possible to pour recipient blocks using ordinary steel molds of different size making the system very flexible. The manufacturing cost for the new device is less than for modified steel molds.

1765 Detecting Clonal T-Cell Populations in Refractory Celiac Sprue and Cutaneous T-Cell Lymphoma: A Comparison of Two TCR Gamma Gene Rearrangement PCR Assays

M Wagner, X Zhu, A Carlin, M Kilgore, S Burkholder, L Houk, AJ Dimarino, J Lee, J Palazzo, T Edmonston. Thomas Jefferson University, Philadelphia, PA.

Background: The detection of clonal T-cell populations in tissue specimens has important diagnostic and prognostic implications for a variety of diseases. In patients with refractory celiac sprue (RCS), the presence of a clonal T-cell population in the small bowel portends a high risk of progression to enteropathy-associated T-cell lymphoma. Detecting a clonal T-cell population in the skin may allow for a more definitive diagnosis of cutaneous T-cell lymphoma (CTCL). We compared the clinical sensitivities of two TCR gamma gene rearrangement (TCR) assays (BIOMED-2 assay and Gene Rearrangement (GR) assay, InVivoScribe) in biopsies of patients with clinically and histologically confirmed RCS and CTCL as well as controls.

Design: DNA was extracted from formalin-fixed, paraffin-embedded tissue sections from 20 skin biopsies and 11 duodenal biopsies. The skin biopsies comprised 9 cases of CTCL, 4 pseudolymphomas (PL), 2 B-cell lymphomas (BCL), and 5 indeterminate cases (IND). The duodenal biopsies comprised 4 cases of RCS, 5 cases of uncomplicated celiac sprue (UCS), and 2 cases of T-cell lymphoma. TCR analysis was then performed using both the BIOMED-2 and the GR assays in duplicate using different amounts of template DNA.

Results: The GR assay detected clonality in 9 skin biopsies (6/9 cases of CTCL, 0/4 PL, 0/2 BCL, and 3/5 IND) and 4 duodenal biopsies (2/4 cases of RCS, 0/5 UCS, and 2/2 cases of T-cell lymphoma). The BIOMED-2 assay detected clonality in 10 skin biopsies (6/9 cases of CTCL, 1/4 PL, 0/2 BCL, and 3/5 IND) and 5 duodenal biopsies (3/4 cases of RCS, 0/5 UCS, and 2/2 cases of T-cell lymphoma). Discrepancies were noted in 3 skin biopsies and 1 duodenal biopsy. 2 CTCLs were positive with one assay but not the other, 1 PL was false positive with the BIOMED-2 assay, and 1 RCS was positive with the BIOMED-2 but not the GR assay.

Conclusions: In this study, the BIOMED-2 assay detected more clonal TCR gamma gene rearrangements than the GR assay in both the skin biopsies and the duodenal biopsies. Given the equivalent clinical sensitivity of both assays for CTCL, the GR assay may be preferable if TCR analysis is needed due to fewer false positive results. The BIOMED-2 assay appears to have a higher clinical sensitivity for RCS than the GR assay and thus may be the preferred assay for these patients due to the prognostic implications.

1766 Automated Double Immunoenzymatic and Colorimetric In-Situ Hybridization Techniques in Evaluation of Immunoglobulin Light Chain Expression

BA Webber, C Cohen. Atlanta VAMC, Decatur, GA; Emory University, Atlanta, GA.

Background: In diagnosis of lymphoid/plasma cell lesions, when flow cytometry results are unavailable, it may be necessary to assess paraffin-embedded fixed tissues to establish B cell/plasma cell clonality. Single color detection based immunohistochemistry for kappa and lambda immunoglobulin light chains is complicated by high background staining, poor sensitivity in non-plasma cell populations, and difficulty identifying particular cell populations in adjacent sections. We compared two commercially available alternative automated methods for evaluating kappa/lambda expression, a double immunoenzymatic (DIE) technique and in-situ hybridization (ISH), in tissues harboring lymphoid or plasma cell lesions processed with B5 (both decalcified and non-decalcified), formalin, and B-plus fixatives.

Design: Single sections of archived paraffin embedded tissues (Emory University, Atlanta, GA) were stained via automated DIE using monoclonal antibodies for kappa and lambda on a Bondmax (Leica) Autostainer and compared with adjacent serial sections stained via automated ISH using pre-diluted kappa and lambda probes on a Ventana Benchmark automated stainer. Cases included 17 plasma cell dyscrasia/myeloma marrows, 1 soft tissue plasmacytoma, 3 diffuse large B cell lymphomas, 2 follicular lymphomas, 6 marginal zone lymphomas, 1 Castleman disease, 1 benign marrow plasmacytosis, and 18 tonsillar lymphoid hyperplasias. All marrows were B5-fixed and decalcified using a hydrochloric acid (HCl) based rapid decalcifying solution, while the remaining cases were processed using formalin, B5, or B-plus fixative. Findings were correlated with previously documented flow cytometric immunophenotyping results.

Results: Correct assessment of clonality was achieved in 33 (66%) and in 28 of 50 (56%) cases by DIE and ISH, respectively. The remaining cases were indeterminate because of absent or poor quality staining. Kappa/lambda expression was only observed in plasma cells, with no reliable staining of lymphoid populations identified by either method. While fixation method had no adverse effect, a large proportion of decalcified specimens yielded non-diagnostic results because of poor quality or absent staining.

Conclusions: DIE and ISH overall are moderately effective methods for evaluating immunoglobulin light chain expression in plasma cells, but these methods demonstrate only limited success in tissues undergoing rapid, HCl-based decalcification.

1767 Use of Digital Slides (DS) for Evaluation of Minimal Disease in Breast Carcinoma: Diagnosis of Microinvasion and of Minute Foci of Carcinoma in Sentinel Lymph Nodes (SLNs)

YH Wen, M Murray, E Brogi. Memorial Sloan-Kettering Cancer Center, New York, NY.

Background: Whole-slide digital scan images provide high morphologic detail. We previously demonstrated good reproducibility in the diagnosis of multiple morphologic variables comparing digital slides (DS) and glass slides (GS) of breast carcinoma. The current study evaluates diagnostic reproducibility in cases with minimal amount of disease, including microinvasive mammary carcinoma (MIC) and small tumor deposits in sentinel lymph nodes (SLNs).

Design: A pathologist (EB) selected a hematoxylin-eosin (H/E) stained slide from each of 9 breast biopsies with question MIC and from 21 SLNs with small amount of disease or lesions mimicking metastatic carcinoma, previously reviewed at our institution (Jan 2003-Aug 2008). Additional material selected for the study included one AE1:AE3-stained slide for each of 12 SLNs, and calponin and p63 stains for 2 biopsies with question MIC. All selected slides were scanned using Aperio ScanScope XT (Aperio Technologies Inc., Vista, CA) at 200x magnification. A pathologist (YHW) blinded to the original diagnosis reviewed first all DS then all GS. The results of DS and GS read were compared and the official diagnosis was used as gold standard. The IRB approved the study.

Results: MIC was present in 7 of 9 biopsies. The study pathologist correctly identified 6 cases of MIC and undercalled the seventh on both DS and GS. A case without MIC was also misdiagnosed on both DS and GS. Of the 21 SLNs, 4 showed clusters <0.2 mm, 4 micrometastases (>0.2 and ≤2 mm), 3 metastases (>2 mm), and 10 had no carcinoma on both H/E and AE1:AE3. The size of the largest tumor cluster ranged between 0.12 and 4.6 mm. Six of the 10 SLNs negative for carcinoma contained lesions that could simulate metastasis, including endosalpingiosis (1), benign ectopic mammary glands (1), necrotizing and non-necrotizing granulomas (2), capsular nevus (1), and silicone lymphadenopathy (1). All non-neoplastic lesions were correctly identified on both DS and GS. There was complete concordance in SLN evaluation obtained using DS, GS, and official diagnosis.

Conclusions: DS provide good morphologic detail, enabling identification of small amount of disease in SLNs, as well as correct diagnosis of some morphologic mimics of metastatic carcinoma. Precise measurement of the tumor clusters is an added benefit of DS. The identification of MIC remains intrinsically more challenging on both DS and GS and accounts for more variable results.

1768 Four Different Molecular Assays for BRAF Mutational Testing: A Sensitivity and Specificity Analysis

B Yang, X Zhang, X Ji, M Jakubowski, JL Hunt. Cleveland Clinic, Cleveland, OH.

Background: Oncogene mutational testing in tumors is becoming important for clinical management of patients with some carcinomas. But, the sensitivity and specificity of different assays to detect somatic point mutations is not well understood. This study compared sensitivity of four different assays for detecting the *BRAF* exon 15 oncogene mutation: gene sequencing, allele specific polymerase chain reaction (ASP), the Mutector kit, and pyrosequencing.

Design: DNA was extracted from microdissected tissue fragments using the High Pure Template Preparation Kit (Roche Applied Science, Indianapolis, IN). A dilution series ranging from 100% BRAF mutant to 1% mutant, diluted in normal DNA, and 15 cases of colon cancer were included in the study. For the gene sequencing, PCR for a 224 basepair product was followed by forward and reverse strand cycle sequencing. ASP was done with fluorescently labeled primers (forward wild-type, forward mutant, and reverse mutant) and analysis performed on the ABI 3730. Pyrosequencing (Biotage Inc. Sweden) was performed on biotinylated PCR products (196 basepair product) with biotinylated forward PCR primer and reverse primer. A reverse primer is used for pyrosequencing. The pyrogram provides percentage and ratio between wild type and mutant alleles The Mutector kit (TrimGen, Sparks, MD) was used according the manufacturer's instructions.

Results: Gene sequencing detected samples where the mutant was present in 25% or more of the sample, with the other three assays detected down to 2% mutant. All 15 patient samples were concordant between these methods (6/15 positive for the BRAF mutation).

Conclusions: Traditional gene sequencing is the least sensitive assay, only detecting mutant when it is present in greater than 25% of the sample. Pyrosequencing, ASP, and the Mutector kits all have excellent sensitivities, yielding interpretable positive results when mutant is present in greater than 2% of the sample. All four methods were equally sensitive and specific for microdissected tissue fragments, which are likely to contain high percentage of tumor cells.

1769 Quantitative Immunofluorescent Assay for Identification of Biomarkers in Formalin-Fixed Mantle Cell Lymphoma Biopsies

DT Yang, BS Kahl, KH Young, JC Eickhoff, AM Petrich, W Huang, CP Leith. University of Wisconsin, Madison, WI.

Background: Identification of prognostic biomarkers is vital in facilitating comparisons across clinical trials and in improving treatment risk stratification. Gene expression profiling (GEP) of mantle cell lymphoma (MCL) has shown over-expression of cell proliferation genes can discriminate between patients with a 6 year median survival difference. However, GEP is currently impractical for clinical use and while immunohistochemistry on formalin-fixed paraffin-embedded (FFPE) tissues has also identified prognostic markers in MCL, limitations in reproducibility and lack of continuous quantification have restricted their clinical application. We assessed the performance of a high throughput assay using automated quantitative analysis (AQUA) of proliferation markers on FFPE on an MCL tissue microarray (TMA).

Design: 20 cases of MCL, diagnosed between 1995 and 2008, were used to construct a TMA with duplicate 1mm cores. Slides were simultaneously stained with DAPI (nuclear mask), anti-CD20 (tumor mask) and 1 of 4 antibodies against proliferation proteins, cdc2, cyclinD1, Ki-67, and mcm2 (targets). Automated quantitative analysis of the target was performed on the AQUA system (HistoRx, New Haven, CT).

Results: AQUA detected a wide range of target expression, particularly of cdc2 and cyclinD1. Results were highly reproducible (>0.70 by intraclass correlation) between duplicate cores. The 25th percentile of the overall survival distribution was 2.7 years. When divided into a poor prognosis group (<3 year survival) and good prognosis group (>3 year survival), two-sample t-test showed a significant difference in cdc2 expression, but not in cyclinD1, Ki-67, or mcm2.

Assessment of proliferation markers by AQUA

Marker	AQUA range	Correlation coefficient	Clinical p-value
cdc2	165-2049	0.82	0.04
cyclinD1	76-2099	0.93	0.66
Ki67	10-40	0.83	0.26
mcm2	51-150	0.71	0.26

Conclusions: On a pilot scale TMA of MCL cases, AQUA demonstrated reproducible continuous quantitation of potential biomarkers and identified an association between cdc2 expression level and patient outcome. Application of TMA/AQUA on a full scale likely has the statistical power and high throughput capabilities to identify prognostic biomarkers in MCL.

1770 Pre-Staining Slides with Hematoxylin for HER-2/neu FISH Testing

A Zarineh, U Krishnamurti, JF Silverman. Allegheny General Hospital, Pittsburgh, PA; Western Pennsylvania Hospital, Pittsburgh, PS.

Background: HER-2/neu testing for invasive breast carcinoma (IBC) is the standard of care. The two common methods of testing are immunohistochemistry (IHC) and fluorescent in situ hybridization (FISH). The advantage of IHC is that the pathologist can microscopically identify the neoplastic cells for interpretation. However, fluorescent in situ hybridization is performed on unstained slides so there may be a question whether the tumor cells are present. We evaluated a new technique of performing HER-2/neu FISH testing in IBC utilizing hematoxylin stained slides.

Design: We selected 23 cases of histologically confirmed IBC that had 2 or 3+ staining for HER-2/neu by IHC and no amplification by FISH. Sections were prepared which was then stained with hematoxylin (H) only to directly visualize the malignant cells to guide the evaluation. The result of FISH on the stained slides was compared to paired unstained slides not undergoing H staining. We also repeated FISH on two cases using previously hematoxylin-eosin (H&E) stained slides to evaluate the interference of background staining. Technical difficulties and interference of faint H staining were also studied.

Results: The fluorescence signal of FISH was not compromised by both H only and standard H&E staining. Comparison of the paired slides showed that the ratio of the amplified to non-amplified increased slightly in 60% (14/23) of the H stained cases, but did not become amplified which was the same result obtained with the traditional unstained slide procedure for FISH Her2/neu analysis. On the two H&E stained slides, one was amplified and one showed no amplification.

Conclusions: We believe this is a valuable new technique to perform FISH testing on H&E and H stained slides. This may be especially helpful when there is extensive necrosis, fibrosis, only a small amount of diagnostic IBC is present and/or when there is the possibility of not having diagnostic IBC in deeper unstained sections of the core needle biopsy submitted for HER-2/neu FISH testing.

1771 PAX-2 as a Renal and Müllerian Tumor Marker. A Comprehensive Study

QJ Zhai, A Ozcan, D Coffey, SS Shen, J Rehana, CR Hamilton, A Kundu, LD Truong. The Methodist Hospital, Houston, TX; Weill Medical College of Cornell University, New York, NY; Gulhane Military Medical Academy and School of Medicine, Ankara, Turkey.

Background: PAX-2 is a transcription factor that is known to promote embryonic differentiation of central nervous system, kidney, and Müllerian organ. PAX-2 has been shown in renal neoplasms and Müllerian-type of neoplasms. However, the diagnostic utility of PAX-2 has not been comprehensively studied.

Design: Formalin-fixed, paraffin-embedded tissue samples for non-neoplastic tissue (443 cases), primary neoplasms (398), and metastatic neoplasms (91) were subjected to immunostain for PAX-2.

Results: PAX-2 was successfully detected as exclusive nuclear staining. For non-neoplastic tissue, PAX-2 was noted focally in glomerular visceral epithelial cells and in a subset of renal collecting ductal cells (89/89); diffusely in atrophic renal tubular epithelial cells (75/75); diffusely in normal endocervical, endometrial, and fallopian tubal cells (19/19), focally in regenerative bile duct epithelium (2/5); focally in lymphoid cell follicles (10/25). PAX-2 was not seen in the rest of tissue samples. For primary neoplasms, PAX-2 was expressed by 1/16 parathyroid adenomas, 1/1 endometrial polyp, 104/ 122 renal cell carcinomas (RCCs), 17/18 renal neoplasms other than RCC, and 9/50 Müllerian-type of neoplasms of ovary or endometrium. PAX-2 was not seen in other neoplasms including 20 transitional cell carcinomas. For metastatic neoplasm, PAX-2 was expressed by 71/95 metastatic RCCs, and 1/20 other metastatic tumors (metastatic endometrioid carcinoma).

Conclusions: Routinely processed tissue is eminently suitable for optimal PAX-2 immunostain. PAX-2 is a marker for Müllerian differentiation, but it is expressed in only a subset of Müllerian tumors. PAX-2 is a marker for renal differentiation and renal tubular atrophy. It is also a very sensitive and specific marker for both primary renal neoplasms and metastatic RCCs.

1772 Three Dimensional Breast Pathology Imaging for Reducing Sampling Errors: A Case Study

JT Zubovits, G Clarke, L Sun, D Wang, A Moskaluk, C Peressotti, M Yaffe. Sunnybrook Health Sciences Centre, Toronto, Canada.

Background: Conventional pathological specimen evaluation may fail to accurately demonstrate tumour extent and closest margin in cases with multifocal or diffuse distribution of disease. These cases include multifocal in-situ ductal carcinoma [DCIS], locally advanced breast cancer [LABC] following neoadjuvant chemotherapy [NAC], or those in which tumor is impalpable (e.g., lobular carcinoma). Positive margins may be missed, the presence of multifocal disease may not be identified, or the tumor size or extent can be underestimated. Secondary treatments may be inadequate and disease can recur.

Design: We developed an efficient method for 3D, whole-specimen histology using whole-mount serial sections and digital imaging techniques. This approach does not require the usual gross sampling techniques, and total fixation and processing time for a mastectomy is a rapid 36 hours. We summarize the technique and present examples to illustrate its clinical utility. We apply the technique to: (1) lobular carcinoma, (2) LABC treated with NAC, 3) multifocal DCIS, and (4) a close or involved margin. To show its potential as a research tool we apply it to study the heterogeneity of biomarkers with established or potential prognostic significance; estrogen receptor and tumour stem cell markers. Digital imaging and display techniques render inspection of a vastly increased amount of histology data feasible.

Results: The specimen preparation and processing techniques yield diagnostic-quality whole-mount serial section images in a feasible timeframe. Comparison between simulated standard sampling technique and the 3D method for two DCIS cases resulted in multifocal disease and an involved margin being identified only with the 3D technique. The full extent of lobular carcinoma was appreciated only using the 3D technique. A more accurate assessment of pathological complete response to chemotherapy can be obtained by applying this technique. Biomarker distribution is readily visualized using whole-mount section images.

Conclusions: The 3D approach is highly amenable for cases which may require more extensive sampling (*e.g.* lobular carcinoma and DCIS, and LABC following NAC) by providing more accurate estimates of margins, or tumour burden when disease is multifocal or diffuse. This new technique allows more accurate tumor measurements and better information regarding the presence and distribution of prognostic and predictive markers.

1773 Application of COLD-PCR for Improved Detection of *KRAS* Mutations in Clinical Samples

Z Zuo, M Soape, S Doan, P Chandra, J Galbincea, B Barkoh, R Luthra. University of Texas MD Anderson Cancer Center, Houston, TX.

Background: *KRAS* mutations, found in 30% of all human tumors, are of prognostic value and can predict response to targeted therapies. Current *KRAS* mutation detection strategy consists of PCR and direct sequencing. To increase detection sensitivity, we evaluated Co-amplification-at-Lower Denaturation-temperature PCR (COLD-PCR) method which selectively amplifies minority mutant alleles, in various types of clinical samples.

Design: The sensitivity and specificity of *KRAS* mutation detection by pyrosequencing after COLD-PCR were compared with that using conventional PCR. Both PCR were performed simultaneously with identical set of primers that amplified a 98 bp region from genomic DNA covering codons 12 and 13 of *KRAS* gene. Based on melting temperature profile, the critical denaturation temperature for COLD-PCR was set to 80 °C versus 94 °C in conventional PCR. Both PCR reactions comprised of 50 cycles. Sensitivities were determined by serial dilution of a positive patient sample in to a negative control. Clinical specimens included bone marrows from 16 leukemia patients and manually microdissected formalin-fixed paraffin-embedded (FFPE) tissue of 28 solid tumors from colon, rectum, liver, lung and bladder.

Results: COLD-PCR increased the sensitivity of *KRAS* mutation detection compared to conventional PCR from 1:8 to 1:32 dilution. In subsequent studies with clinical specimens, COLD-PCR successfully detected mutations in all samples that were positive by conventional PCR, and enhanced the mutant to wild-type ratio by 2 to 3 folds. In a leukemia follow up bone marrow, COLD-PCR detected a mutation that was missed by conventional PCR. The enhancement of mutation detection by COLD-PCR inversely correlated with the tumor cell percentage in the samples. Higher enhancement was observed in FFPE samples than in bone marrow specimens. Implementation of the method was straightforward, requiring no additional cost for reagents and instruments. The method maintained high specificity and reproducibility.

Conclusions: Our study showed that COLD-PCR increased the *KRAS* mutation detection sensitivity from 6% to 1.5% in comparison to conventional PCR methods. This method is especially beneficial for clinical applications in solid tumors due to more prominent enhancement of mutation detection in FFPE samples. COLD-PCR may not only reduce repeat testing due to equivocal results in specimens that have low percentage of tumor cells in high non-neoplastic background but also find utility in monitoring therapy response.

Ultrastructural

1774 Dense Deposit Disease Mimicking Acute Post-Infectious Glomerulonephritis

J Hicks, D Kelly, E Mroczek-Musulman, S Goldstein, K Eldin. Texas Children's Hospital & Baylor College of Medicine, Houston, TX; Children's Hospital & University of Alabama, Birmingham, AL.

Background: Dense deposit disease (DDD) has been recently reviewed (Mod Pathol 2007:20:606-16) with the conclusion that DDD is a distinct entity separate from membranoproliferative disease. DDD demonstrates 5 patterns: 1) membranoproliferative; 2) mesangial proliferative; 3) crescentic; 4) acute proliferative/exudative; 5) unclassified. Crescentic and acute proliferative/exudative patterns occurred between 3 and 18 years of age. While other DDD patterns had a wide age range (3-67yrs) with 90% occurring in those ≤30 years of age. DDD disease may mimic acute post-infectious glomerulonephritis (AGN) on light, immunofluorescence (IF) and electron microscopy (EM).

Design: DDD (crescentic and acute proliferative/exudative patterns) mimicking AGN on initial presentation were identified in 6 patients at 2 pediatric hospitals (3M:3F, age range 4-12 yrs; AGN symptoms: hematuria, proteinuria, elevated Cr). Following medical